VTRC
Virginia Transportation Research Council

We Bring Innovation to Transportation

Experimental and Analytical Evaluation of Residual Capacity of Corrosion-Damaged Prestressed Concrete Bridge Girders

https://vtrc.virginia.gov/media/vtrc/vtrc-pdf/vtrc-pdf/25-R18.pdf

ALI H. ALFAILAKAWI, Assistant Professor
Public Authority for Applied Education and Training

C.L. ROBERTS-WOLLMANN, Ph.D., P.E., Professor
Via Department of Civil and Environmental Engineering
Virginia Tech

IOANNIS KOUTROMANOS, Ph.D., Associate Professor
Via Department of Civil and Environmental Engineering
Virginia Tech

MATTHEW HEBDON, Ph.D., P.E., Associate Professor
Department of Civil and Environmental Engineering
Utah State University

Final Report VTRC 25-R18

VIRGINIA TRANSPORTATION RESEARCH COUNCIL
530 Edgemont Road, Charlottesville, VA 22903-2454
vtrc.virginia.gov

Standard Title Page—Report on State Project

Report No.: VTRC 25-R18	Report Date: April 2025	No. Pages: 67	Type Report: Final Contract	Project No.: 114590
			Period Covered:	Contract No.:

Title:
Experimental and Analytical Evaluation of Residual Capacity of Corrosion-Damaged Prestressed Concrete Bridge Girders

Key Words:
prestressed concrete, flexural strength, residual strength, corrosion, damage,

Author(s):
Ali Alfailakawi, C. L. Roberts-Wollmann, Matthew Hebdon, and Ioannis Koutromanos

Performing Organization Name and Address:

Virginia Transportation Research Council 530 Edgemont Road Charlottesville, VA 22903	Virginia Tech Dept of Civil Engineering Blacksburg, VA

Sponsoring Agencies' Name and Address:
Virginia Department of Transportation
1401 E. Broad Street
Richmond, VA 23219

Supplementary Notes:

Abstract:

The durability of infrastructure components, such as prestressed concrete bridge beams, can be significantly affected by long-term deterioration associated with corrosion. Corrosion is a major concern for bridges in Virginia, due to the frequent use of deicing salts during the winter, as well as the number of structures in marine environments. The residual capacity of corrosion damaged prestressed I-beams and box beams needs to be accurately estimated to determine if damaged bridges need to be posted, and to help with making informed decisions related to repair, rehabilitation and replacement of damaged bridges.

This report presents the results of testing of six corrosion-damaged prestressed beams removed from existing bridges during their demolition. Three beams were Type II AASHTO I-beams extracted from the Lesner Bridge in Virginia Beach, and three were 48 in wide by 27 in deep box beams extracted from the Aden Road Bridge near Quantico, Virginia. Prior to testing, the beams were visually inspected and two types of non-destructive evaluations were performed to identify corrosion activity: resistivity measurements and half-cell potential measurements. The beams were then tested in the lab to determine their flexural strength. Following testing, samples of strand were removed and tested to determine their tensile properties. Cores were taken from the Aden Road beams and from both the beams and decks of the Lesner Bridge beams to determine compressive strength. Powdered concrete samples were removed to perform chloride concentration tests.

The tested strengths of the beams were compared to calculated strengths using two methods for damage estimation and two different calculation approaches. The methods for damage estimation relied exclusively on visual inspections; one was the set of methods recommended by Naito et al. (2010), while the second was a modified method developed in this study from the current tests. The two calculation approaches were a strain compatibility method and the AASHTO LRFD method. Overall, the results yielded reasonable estimates of residual strength, except for one of the box beams that was discovered to have considerable water within the hollow cells. The final recommendations are that bridge inspectors develop detailed damage maps of corrosion-damaged beams, and that load raters use the Naito et al. method to get a conservative estimate of damage for both box beams and I-beams. Either method for calculating strength is valid, however the AASHTO LRFD method is simpler.

FINAL REPORT

EXPERIMENTAL AND ANALYTICAL EVALUATION OF RESIDUAL CAPACITY OF CORROSION-DAMAGED PRESTRESSED CONCRETE BRIDGE GIRDERS

Ali H. Alfailakawi
Assistant Professor
Public Authority for Applied Education and Training

C.L. Roberts-Wollmann, Ph.D., P.E.
Professor
Via Department of Civil and Environmental Engineering
Virginia Tech

Ioannis Koutromanos, Ph.D.
Associate Professor
Via Department of Civil and Environmental Engineering
Virginia Tech

Matthew Hebdon, Ph.D., P.E.
Associate Professor
Department of Civil and Environmental Engineering
Utah State University

Project Manager
Bernard L. Kassner, Ph.D., P.E.
Virginia Transportation Research Council

Virginia Transportation Research Council
(A partnership of the Virginia Department of Transportation
And the University of Virginia since 1948)

Charlottesville, Virginia

April 2025

VTRC 25-R18

DISCLAIMER

The project that is the subject of this report was done under contract for the Virginia Department of Transportation, Virginia Transportation Research Council. The contents of this report reflect the views of the author(s), who is responsible for the facts and the accuracy of the data presented herein. The contents do not necessarily reflect the official views or policies of the Virginia Department of Transportation, the Commonwealth Transportation Board, or the Federal Highway Administration. This report does not constitute a standard, specification, or regulation. Any inclusion of manufacturer names, trade names, or trademarks is for identification purposes only and is not to be considered an endorsement.

Each contract report is peer reviewed and accepted for publication by staff of Virginia Transportation Research Council with expertise in related technical areas. Final editing and proofreading of the report are performed by the contractor.

ABSTRACT

The durability of infrastructure components, such as prestressed concrete bridge beams, can be significantly affected by long-term deterioration associated with corrosion. Corrosion is a major concern for bridges in Virginia, due to the frequent use of deicing salts during the winter, as well as the number of structures in marine environments. The residual capacity of corrosion damaged prestressed I-beams and box beams needs to be accurately estimated to determine if damaged bridges need to be posted, and to help with making informed decisions related to repair, rehabilitation and replacement of damaged bridges.

This report presents the results of testing of six corrosion-damaged prestressed beams removed from existing bridges during their demolition. Three beams were Type II AASHTO I-beams extracted from the Lesner Bridge in Virginia Beach, and three were 48 in wide by 27 in deep box beams extracted from the Aden Road Bridge near Quantico, Virginia. Prior to testing, the beams were visually inspected and two types of non-destructive evaluations were performed to identify corrosion activity: resistivity measurements and half-cell potential measurements. The beams were then tested in the lab to determine their flexural strength. Following testing, samples of strand were removed and tested to determine their tensile properties. Cores were taken from the Aden Road beams and from both the beams and decks of the Lesner Bridge beams to determine compressive strength. Powdered concrete samples were removed to perform chloride concentration tests.

The tested strengths of the beams were compared to calculated strengths using two methods for damage estimation and two different calculation approaches. The methods for damage estimation relied exclusively on visual inspections; one was the set of methods recommended by Naito et al. (2010), while the second was a modified method developed in this study from the current tests. The two calculation approaches were a strain compatibility method and the AASHTO LRFD method. Overall, the results yielded reasonable estimates of residual strength, except for one of the box beams that was discovered to have considerable water within the hollow cells. The final recommendations are that bridge inspectors develop detailed damage maps of corrosion-damaged beams, and that load raters use the Naito et al. method to get a conservative estimate of damage for both box beams and I-beams. Either method for calculating strength is valid, however the AASHTO LRFD method is simpler.

FINAL REPORT

EXPERIMENTAL AND ANALYTICAL EVALUATION OF RESIDUAL CAPACITY OF CORROSION-DAMAGED PRESTRESSED CONCRETE BRIDGE GIRDERS

Ali Alfailakawi, Graduate Research Assistant

C.L. Roberts-Wollmann, Ph.D., P.E., Professor

Matthew Hebdon, Ph.D., P.E., Assistant Professor

Ioannis Koutromanos, Ph.D., Associate Professor

Via Department of Civil and Environmental Engineering, Virginia Tech

INTRODUCTION

Background

The durability of infrastructure components such as bridges is significantly affected by long-term deterioration associated with corrosion. The transport of agents and the chemical processes associated with corrosion lead to cracking in the concrete, which then accelerates the corrosion process. Corrosion is a significant concern for bridges in Virginia, due to the frequent use of deicing salts during the winter, as well as the number of structures in marine environments. Over time, the exposure of prestressing steel to corrosive agents can lead to complete loss of strands and, in extreme circumstances, to complete failure of bridge beams (Naito et al. 2010). Research is necessary to assess the impact of corrosion on the local and global behavior of bridges and to establish mitigation techniques to ensure long-term durability.

At present, there is a relatively limited amount of experimental research on bridge girders damaged by corrosion. Researchers in New Zealand, Japan and Pennsylvania have conducted destructive tests on decommissioned prestressed beams (Rogers et al. [2012], Harries [2009] and Tanaka et al. [2012]); however, these members may not be representative of the design and construction practice in Virginia. A comprehensive research program was carried out by Naito et al. (2010) to study corrosion-damaged precast, prestressed adjacent box beams with the objective of developing guidelines for the calculation of residual strength based on visual inspections. They collected beams from demolished bridges and performed forensic investigations. No physical tests were performed as part of this program to determine actual flexural strength, although a previous research program (Harries, 2009) tested two beams from an adjacent box beam bridge. Based on excavating strands from the beams, Naito et al. determined that the probability of corrosion damage was highest for strands located beneath a longitudinal crack. There was also a higher probability of corrosion for strands immediately adjacent to the strand beneath the crack. Based on proximity to cracks or spalls, they made recommendations for a reduced cross-sectional area to be used in strength calculations. In the project presented herein,

additional data was collected to enhance the recommendations made by Naito et al. (2010), and also go a step further by testing the beams to failure to validate the approach.

Problem Statement

A method to determine the capacity of prestressed concrete members with section loss and corrosion of prestressing strands is not well-established. The understanding of the residual capacity is critical for the evaluation of bridges with advanced levels of deterioration.

PURPOSE AND SCOPE

Purpose

The overall purpose of this study was to conduct tests to determine the remaining capacity of prestressed concrete members, which have localized regions of deterioration, and develop a method that can be used to determine the residual capacity of prestressed concrete bridge beams based primarily on visual inspections. These tests should aid in the development of guidelines for inspectors to insure they collect the necessary data on damage to aid in the calculation of strength for load rating.

Scope

In order to achieve the objective of this project, three adjacent prestressed concrete box beams and three prestressed I-beams were tested to failure to determine their residual flexural capacity after many years of service. These beams, retrieved from bridges that were being demolished, had varying degrees of deterioration, ranging from delaminated concrete to strands with severe section loss. Prior to testing damage was mapped and non-destructive evaluations were performed. After testing samples of strand, concrete cores, and powdered concrete samples were removed and tested.

METHODS

Visual Inspection, Damage Mapping and Selection of Beams to Be Tested

Six corrosion-damaged beams were tested in this research project. Three were prestressed I-beams from the Lesner Bridge in Virginia Beach, and three were prestressed box beams from the Aden Road Bridge near Quantico, Virginia. This section provides general information about the beams, damage map creation and selection of the beams to be tested.

Lesner Bridge Beams

The west bound lanes of the Lesner Bridge, also known as the Lynnhaven Inlet Bridge, were constructed in 1967. The structure comprised prestressed concrete beams in the approaches

and steel beams for the main spans. The beams in the approach spans were 49 ft – 9 in long, 36 in deep prestressed I-beams. The beams were specified to have 5000 psi concrete and were prestressed with 22 7/16-in Grade 270 stress-relieved prestressing strands. There were seven beams in each span, spaced at 5 ft – 2.5 in, center-to-center.

After almost 50 years of service, the bridge was demolished and replaced beginning in 2016. In the spring of 2017, nine beams were retrieved during the demolition process and delivered to Virginia Tech for testing. The slab between the beams was saw-cut to allow for the retrieval of beams to include a section of their cast-in-place composite deck. Figure 1 is a photograph of Span 7, showing the extent of deterioration in typical beams. The Lesner Bridge was repaired several times over the years, so patching is evident in many locations.

Figure 1. Typical Deterioration on the Lesner Bridge

For simplification purposes, the Lesner Bridge beams in this report will be referenced by I-Beam 1 through I-Beam 9. Table 1 presents the beam designations and their original locations in the bridge.

Table 1. Alternative Names for Lesner Bridge Beams

Girder #	Girder Designation on Bridge
I-Beam 1	Span 22 Beam 5
I-Beam 2	Span 7 Beam 2
I-Beam 3	Span 19 Beam 4
I-Beam 4	Span 22 Beam 2
I-Beam 5	Span 19 Beam 2
I-Beam 6	Span 11 Beam 4
I-Beam 7	Span 13 Beam 5
I-Beam 8	Span 7 Beam 4
I-Beam 9	Span 5 Beam 2

Aden Road Bridge Beams

The Aden Road Bridge was constructed in 1979. It was a three-span bridge with nine prestressed box beams per span. The fascia beams were 3 ft – 0 in wide by 27 in deep, and the

seven interior beams were 4 ft – 0 in wide by 27 in deep. Only interior beams were used in this project. The beams were 55 ft long and were prestressed with 33 7/16-in diameter Grade 270 stress relieved strands. The beams were connected transversely with grouted 12-in deep shear keys, and ½-in diameter Grade 270 prestressing strands at each quarter point of each span. The bridge had an asphalt wearing surface applied directly to the top of the box beams, which was removed prior to demolition of the bridge.

After slightly over 30 years of service, the joints had failed and the bridge was showing signs of severe deterioration, including exposed and fractured prestressing strands (see Figure 2). In 2013, the bridge was demolished and replaced. During demolition, six of the interior beams were transported to Virginia Tech for future testing, three of which were tested in this project. The Aden Road Bridge beams will be referenced by the names Box Beam 1 through Box Beam 6, but their original positions in the bridge is unknown.

Figure 2. Typical Corrosion Damage on Aden Road Bridge

Visual Inspection and Damage Mapping

The nine Lesner and six Aden Road beams were examined and each beam's existing condition was thoroughly documented. The documentation included the location of damage such as cracks, delaminations, spalling, section loss and strand exposure. Delaminations were located by tapping the sides of the beams with a hammer and recording locations that had a hollow or dead sound. Detailed damage maps were created for each beam, indicating the size and location of each defect. The goal was to select three beams from each bridge: one with little damage, one with a moderate amount of damage and one with severe damage.

Selection of Beams to Be Tested

To aid in the selection, a method was established to quantify and evaluate the condition of the beams, and a grading system was established. This grading system had a total of three steps. First, four types of defects in the girders were measured: the total longitudinal cracking, total amount of section loss in the concrete, total amount of delaminated area, and total amount of patched area. The total longitudinal cracking is the sum of the lengths of all of the cracks

within a beam. The total amount of section loss is the sum of each section loss, by surface area, observed in a girder. This applies for both delaminated and patched areas. Second, for each defect type, the measurements for each beam were compared to the worst recorded measure of that defect amongst all of the girders. Third, a weighting factor was applied to each damage measure. The factors used for this system were 0.15 for the patched area defect, 0.3 for longitudinal cracking, 0.2 for delamination, and 0.35 for amount of section loss. The weighting factors were somewhat arbitrary, but generally based on the findings of Naito et al. (2010), where longitudinal cracking indicated the strand beneath the crack and adjacent to the crack had a high probability of corrosion damage. So, longitudinal cracking got a relatively high weight. Similarly, spalling and delaminations were also evidence of corrosion. It was often uncertain what damage was present underneath a patch, so its weighting factor was somewhat lower. This method is not meant to be used in bridge evaluation in general, but rather was developed for the purposes of ranking the salvaged beams to determine which would be tested for this study and to reserve beams with certain levels of deterioration for a future study.

Using this information, a comparison between the available beams was made to categorize them with respect to the conditions. Each type of damage was quantified for each beam, and each type of damage was given a weighting factor. The sum of each beam's damage multiplied by its factor was determined. Then a beam with very low damage, one with medium damage and one with extreme damage (i.e., those beams in "good", "medium", and "poor" condition), from each bridge, were selected for further testing.

Unfortunately, the six box beams transported to Virginia Tech from the Aden Bridge could not be assessed prior to transport. So, unlike the Lesner Bridge girders, the decision was to rate the first three box beams brought to the lab as "good", "medium", and "poor.'' All nine Lesner Bridge beams were evaluated to determine the three that would be used in this phase of the research program.

Non-Destructive Evaluations

Concrete Resistivity Test

The concrete resistivity is primarily affected by two factors: the concrete quality and moisture content. The higher the moisture content is, the lower the resistivity is. Results obtained from the resistivity test do not indicate whether the reinforcing steel is corroded or not. Rather, they give additional information about the locations which exhibit the conditions that may result in a high corrosion rate. In this study, the concrete resistivity was determined using a four-point Wenner probe as per AASHTO-T-358 (2015), where a current was applied to the two outer probes, and the potential difference was measured between the two inner probes. A grid similar to the one shown in Figure 3 was used to obtain the resistivity measurements on I-Beam 7 from the Lesner Bridge; however, the measurements for this test were at 6-in intervals, versus the 12-in intervals in Figure 3. Due to difficulties with this test, as discussed in the *Results* section, no other I-beams and none of box beams were tested for resistivity.

Half-Cell Potential

The half-cell potential method provides a fast, cost-effective, and non-destructive method to predict the corrosion in concrete by mapping the potential corrosion of the strands and mild reinforcement along the beam. The basic premise of the half-cell was to measure the potential difference between the steel and a standard copper sulfate electrode on the concrete surface. This measurement was made by placing the electrode on the embedded steel under the concrete cover. The reading of the potential difference was displayed in a voltmeter. The more negative the voltage the more likely that corrosion was present at the measured location. The measurement and procedures were based on ASTM C876 standards (2015).

The sides of these beams were marked with a grid, as shown in Figure 3. Each strand on the three I-beams from the Lesner Bridge was assigned a number as shown in Figure 4. Likewise, Figures 5 and 6 show the grid and strand numbering system, respectively, for the Aden Road Bridge box beams. To collect complete data, the voltmeter was connected to a single strand, and measurements were taken at all grid intersection points on both sides of the beam. These measurements were repeated for each strand on each beam.

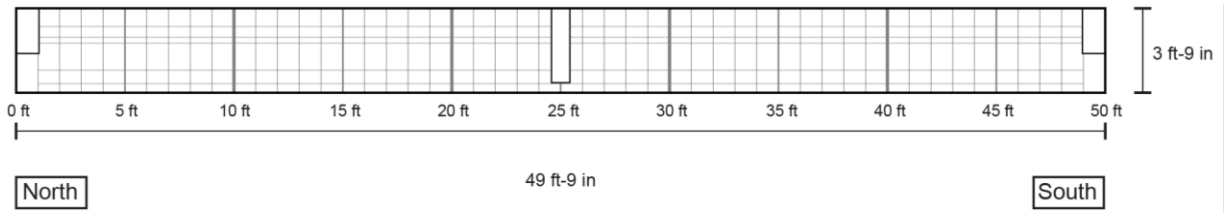

Figure 3. Grid Marked on Lesner Bridge I-Beams for Half Cell Potential Testing.

Tests to Determine Flexural Strength

Test Set Up

All six of the selected beams were tested in a simple-span configuration with a roller support at one end and a pin support at the opposite end. Loads were applied with a 400-kip actuator and a spreader beam, so two equal loads were applied 8 ft apart, centered at the mid-span of the beam. Preliminary strength calculations were performed for each beam prior to testing to confirm a flexural failure would occur prior to a shear failure. Figure 7 presents a schematic of the test setup for the Lesner Bridge I-beams and Figure 8 shows the setup for the Aden Road Bridge box beams.

Instrumentation

Each flexural test had similar instrumentation. Wire pots were used to measure the vertical deflections at the mid-span and quarter points. BDI gages were used to measure longitudinal strains at several locations along the length of the beam. At each location, an array of BDI gages was installed vertically, through the depth of the beam, to investigate strain distributions and to determine the location of the centroid of the cross-section. A load cell was

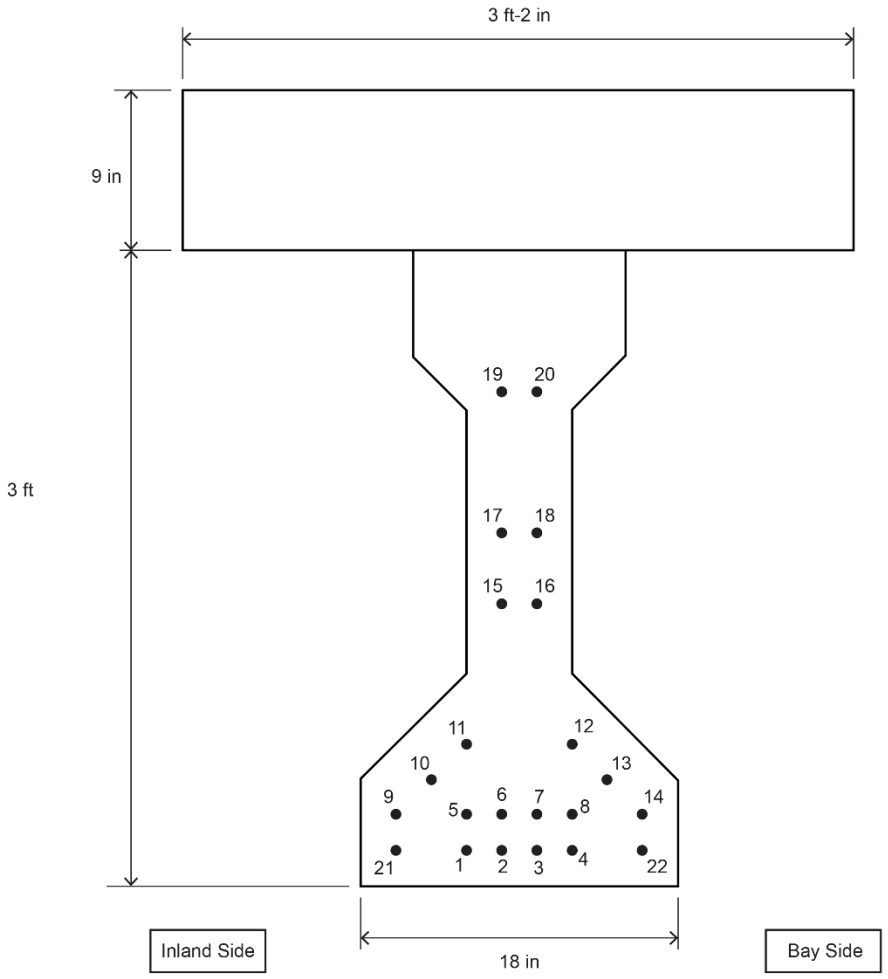

Figure 4. Strand Numbering for Lesner Bridge I-Beams for Half Cell Potential Testing

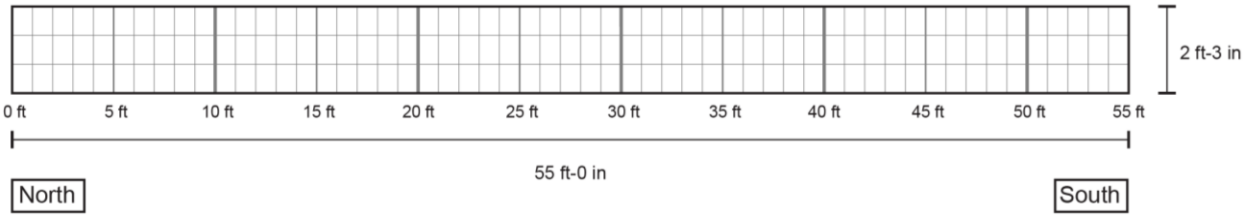

Figure 5. Grid Marked on Aden Road Bridge Box Beams for Half Cell Potential Testing.

placed between the hydraulic ram and the cross-head of the loading frame. The load cell, wire potentiometers and the BDI strain transducers were connected to a wireless BDI data acquisition system. The system sampled the data at a rate of 33 HZ throughout testing. Figure 9 is a schematic of the BDI gage arrangement for the Lesner Bridge I-beams and Figure 10 is a schematic of the BDI gage arrangement for the Aden Road Bridge box beams.

Test Procedure

For each beam, an expected cracking load was calculated prior to testing. During testing, the load was increased in 5- or 10-kip increments to slightly below this expected load. After

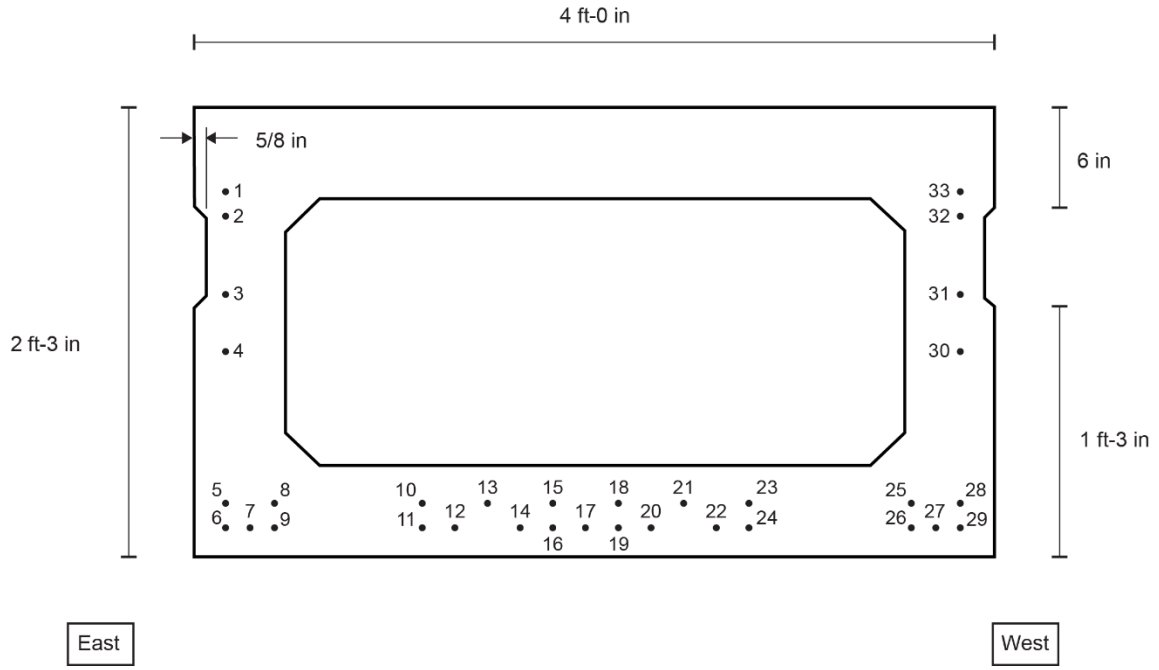

Figure 6. Strand Numbering for Aden Road Box Beams for Half Cell Potential Testing

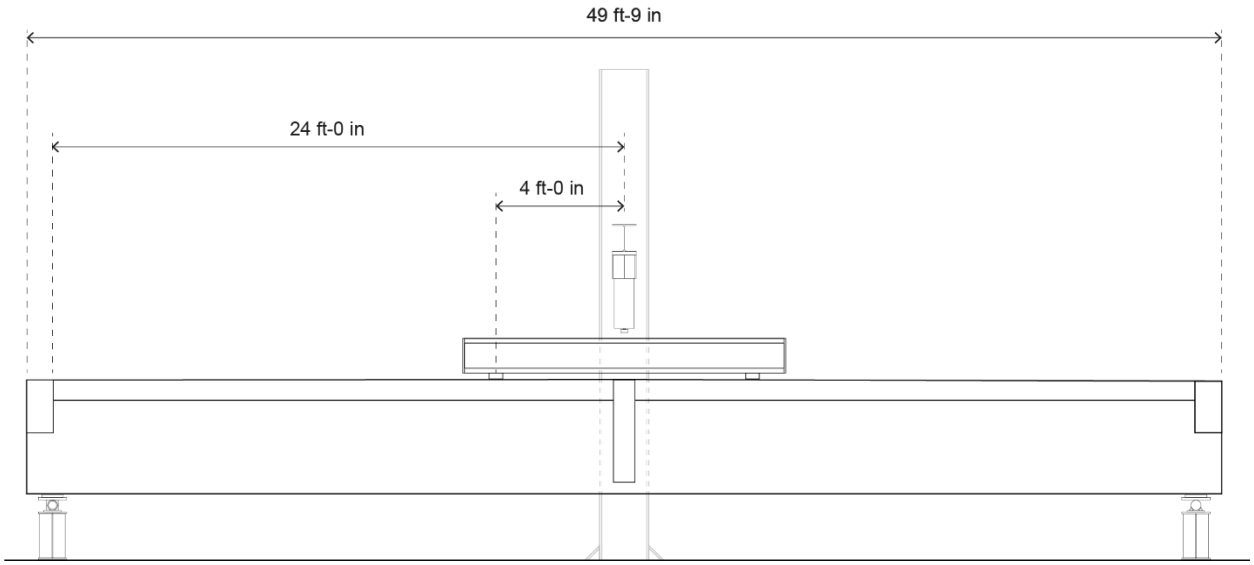

Figure 7. Flexural Testing Setup for Lesner Bridge I-Beams

each subsequent load increment, all cracks were marked and photographs taken. After the beam began to exhibit signs that the prestressing was yielding and the load was not increasing significantly, loading protocol was changed to a manual deflection control. An increment of deflection was chosen based on the load-deflection behavior at that point of the testing. At each increment, the load was paused and the beam was examined. When failure appeared imminent, the researchers did not continue to approach the beam to look for new cracks or crack propagation. Loading continued until failure occurred, due either to top flange crushing or due to the beam continuing to deform without resisting any additional load.

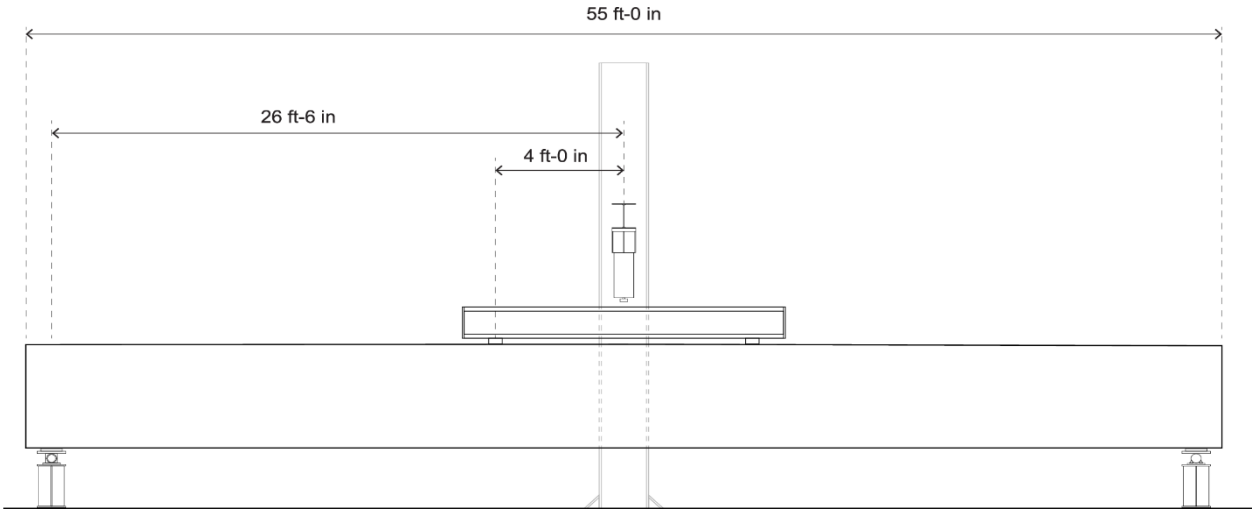

Figure 8. Flexural Testing Setup for the Aden Road Bridge Box Beams

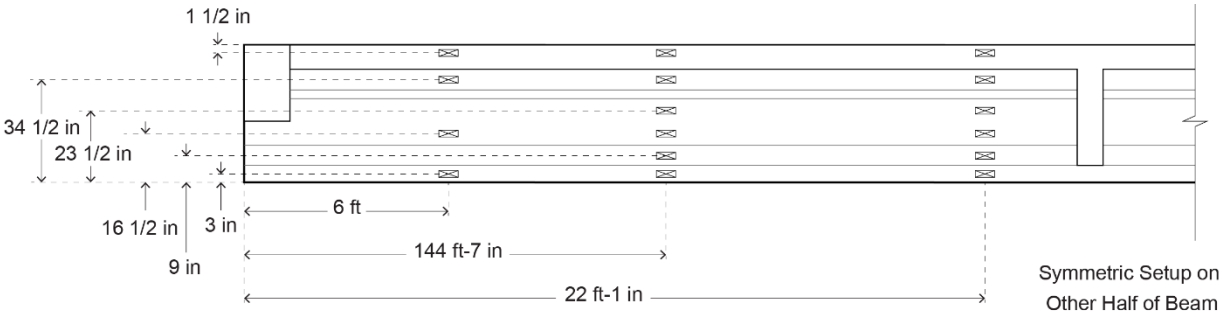

Figure 9. Locations of BDI Gages on Lesner Bridge I-Beams

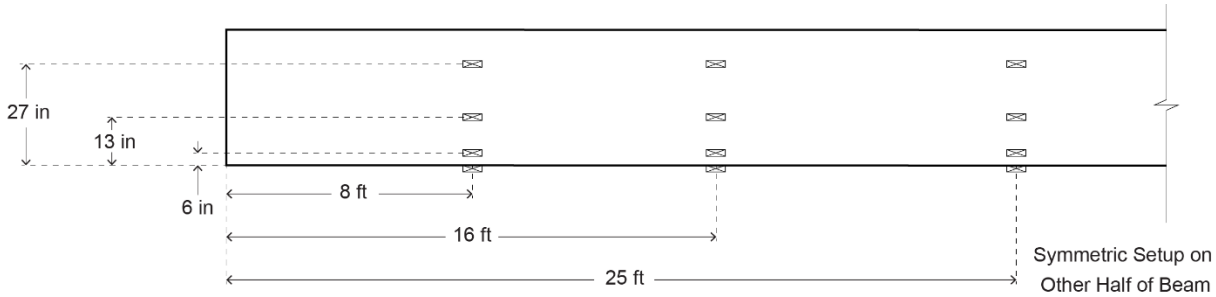

Figure 10. Locations of BDI Gages on the Aden Road Bridge Box Beams

After failure, the load was removed and the beam was carefully examined to determine the number of prestressing strands that either showed evidence of having been fractured due to corrosion prior to testing or had failed during testing.

Post-Test Destructive Testing

Total Chloride Evaluation

ASTM C1152 (2012) method was used to assess the acid soluble chloride profiles using a 10-g sample of pulverized concrete that should be able to pass a fine sieve. This method allows

the use of potentiometric titration to determine the chloride content in a given sample. Samples of concrete were collected from each side of each beam, as shown in Figures 11 through 16. Beams are presented in order of their relative grade based on visual inspection: good, medium, bad (see the *Results* section). For the Lesner Bridge I-beams, samples were taken on both sides, the side that faced the bay when the beam was in the bridge and the side that faced inland. Also, two samples were taken from each side, one from the horizontal face (perpendicular to the bottom face) and one from the inclined face of the bottom flange. The bay side typically had more damage than the side that faced inland.

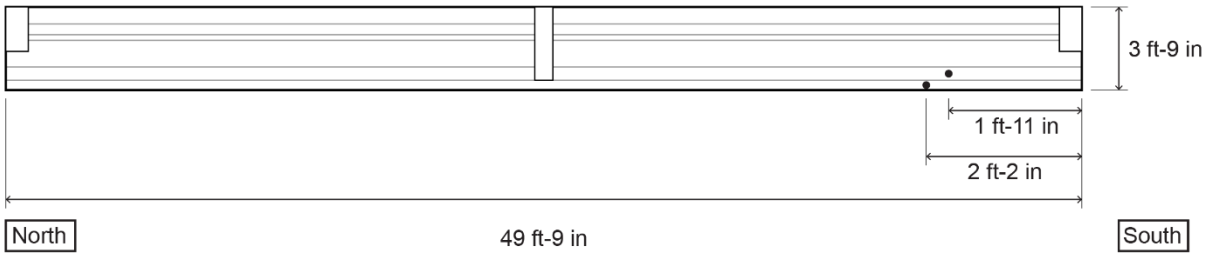

Figure 11. Locations of Chloride Samples Taken from I-Beam 7 – Good Condition

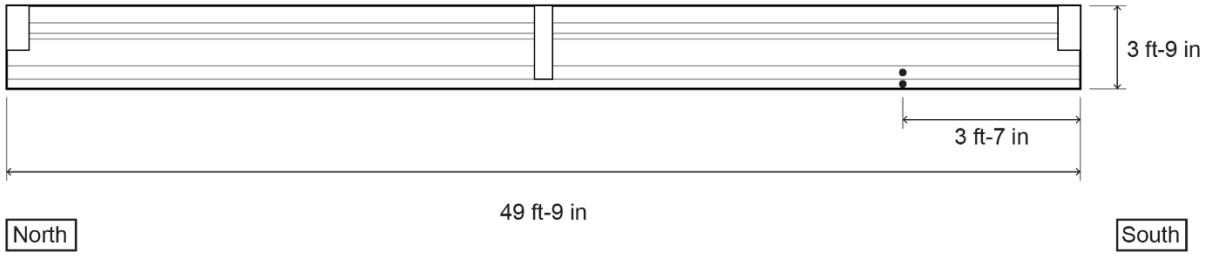

Figure 12. Locations of Chloride Samples Taken from I-Beam 6 – Medium Condition

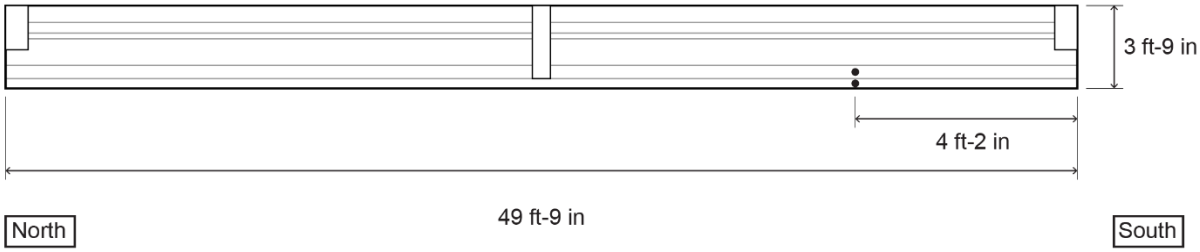

Figure 13. Locations of Chloride Samples Taken from I-Beam 3 – Bad Condition

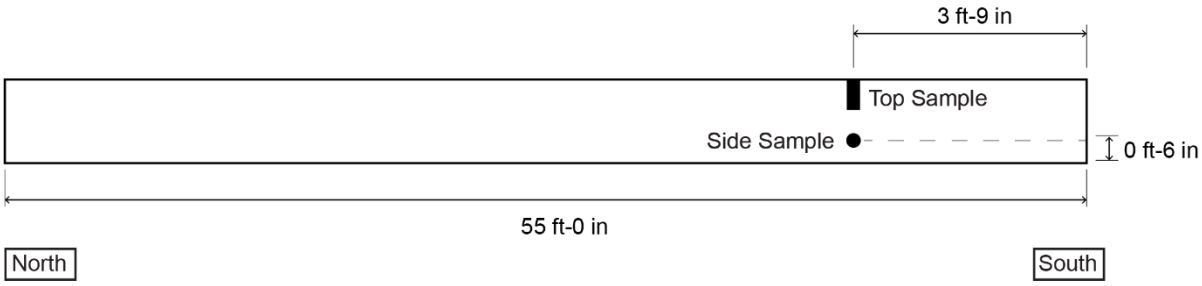

Figure 14. Locations of Chloride Samples Taken from Box Beam 1 – Good Condition

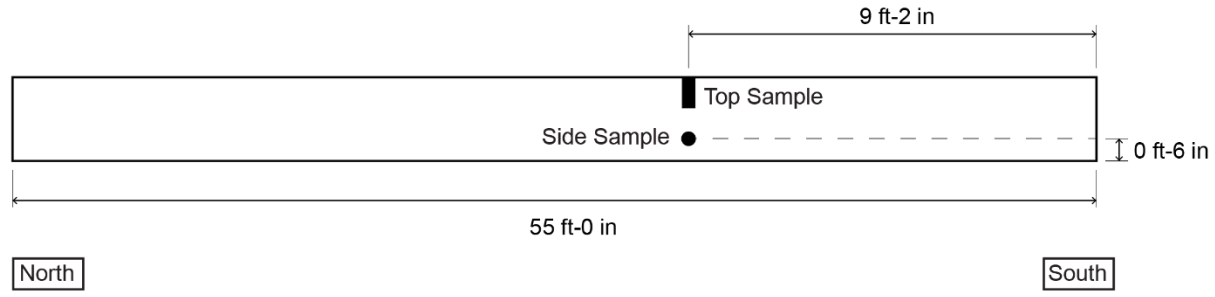

Figure 15. Locations of Chloride Samples Taken from Box Beam 4 – Medium Condition

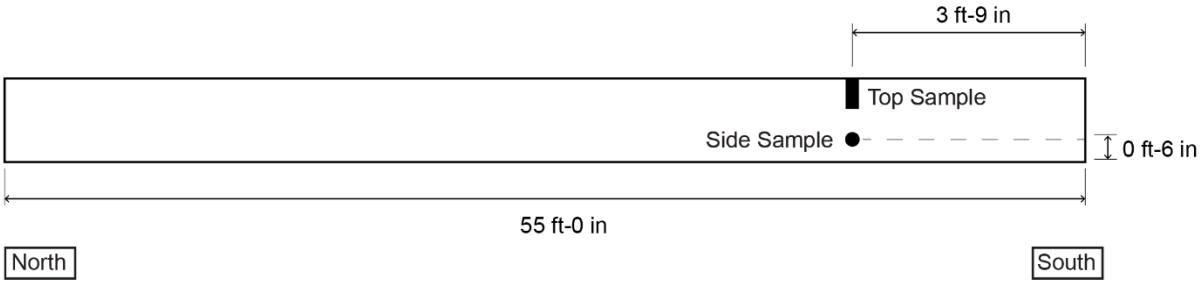

Figure 16. Locations of Chloride Samples Taken from Box Beam 2 – Bad Condition

One-hundred eleven samples were collected from the six beams. A drill with a 1-in diameter drill bit was used at selected locations on each beam to collect powdered samples of concrete. Locations were selected based on being in sound concrete, not damaged by testing, and away from reinforcing bars as determined using a hand held GPR. For each location, the first 0.25-in depth of concrete was discarded and then powdered samples were collected in increments of 0.5 in for a minimum depth of 2 in down to the level of the strands. During drilling, the powder sample was collected using a coffee filter and vacuum. Then, the sample was secured in clean dry plastic bag.

Compression Strength Testing

To determine the compressive strength of the beams of both bridges and the sections of the cast-in-place composite deck that remained attached to the I-beams of the Lesner Bridge, core sample testing was done in accordance with ASTM C39 (2005). Core samples for each beam were obtained following ASTM C42 (2016).

For this project, nineteen core samples were drilled in total. Two cores from the beams and two from the decks were taken from each of the three Lesner Bridge Beams. Two cores were taken from two box beams and three from the third. The location of each sample is shown in Figures 17 to 22. A coring rig and hand drill were used to obtain the cores. The distinction between the two is that the rig was used to get vertical cores while the hand drill was used to get horizontal cores. Also, different bit diameters were used depending on the spacing between the reinforcing bars.

After each core was removed, the researchers measured the length and diameter of the specimen. If the ratio of the length to the diameter was equal or less than 1.75, a strength

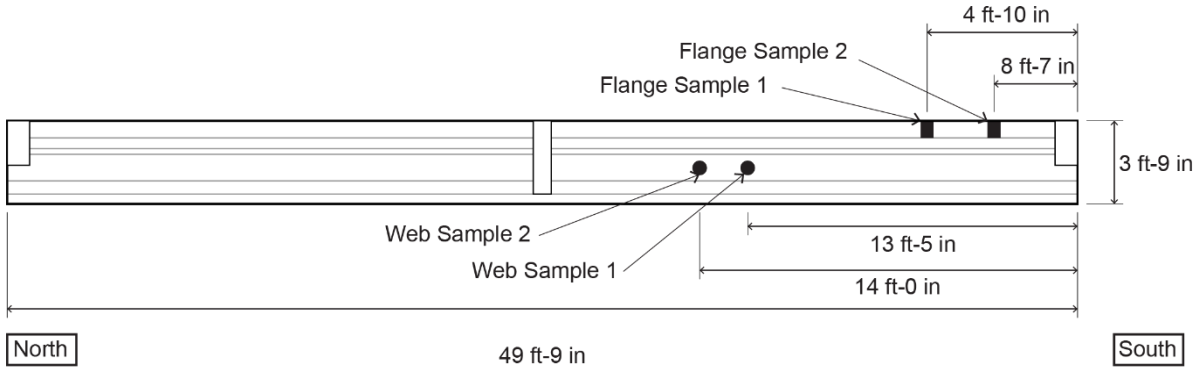

Figure 17. Location of Cores Taken from I-Beam 7. Elevation view of beam is shown.

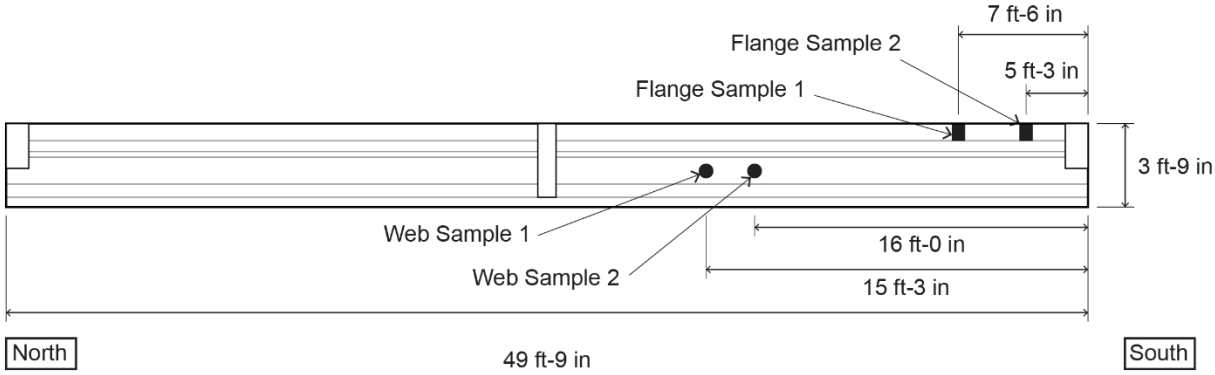

Figure 18. Location of Cores Taken from I-Beam 6. Elevation view of beam is shown.

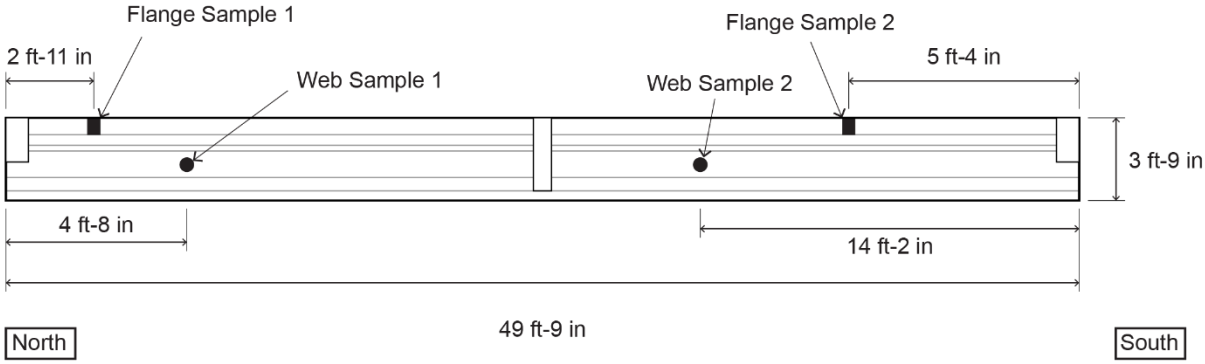

Figure 19. Location of Cores Taken from I-Beam 3. Elevation view of beam is shown.

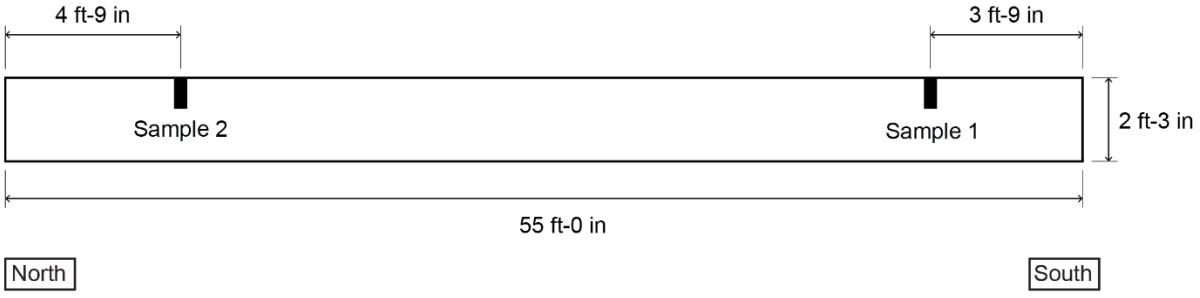

Figure 20. Location of Cores Taken from Box Beam 1. Elevation view of beam is shown.

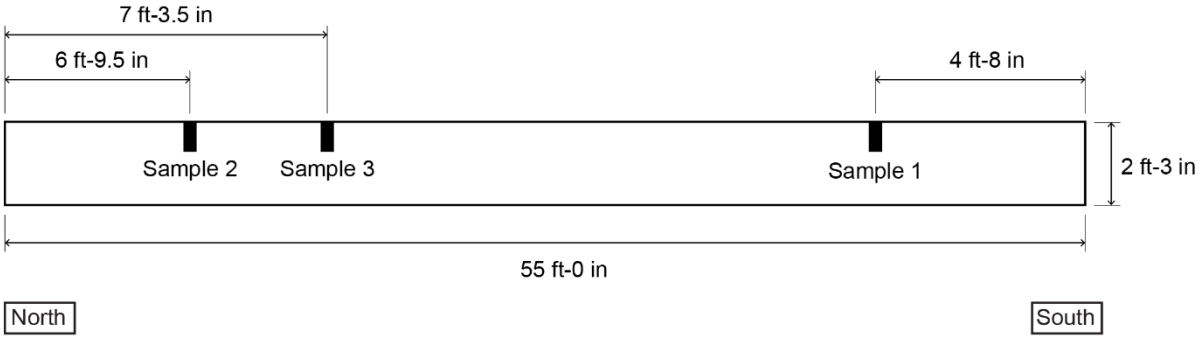

Figure 21. Location of Cores Taken from Box Beam 4. Elevation view of beam is shown.

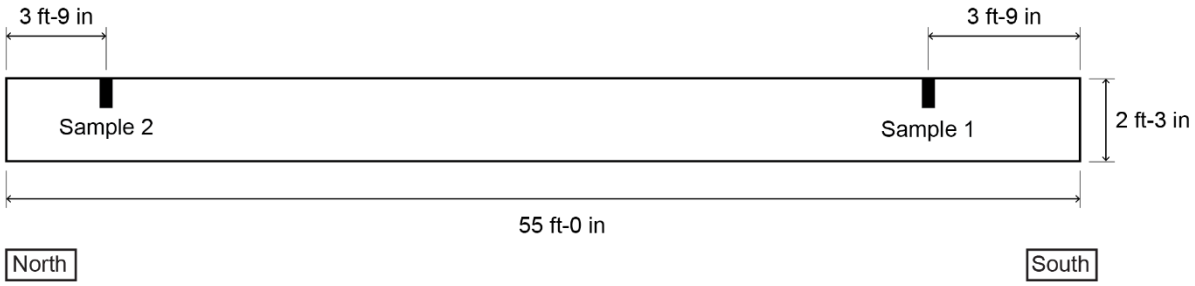

Figure 22. Location of Cores Taken from Box Beam 2. Elevation view of beam is shown.

correction factor (shown in Table 2) adjusted the compressive strength of the core sample determined from the ASTM C39 test.

Table 2. Strength Correction Factor

Ratio of Length to Diameter (L/D)	Strength Correction Factor
1.75	0.98
1.50	0.96
1.25	0.93
1.00	0.87

Tension Tests of Retrieved Strands

After the completion of flexural tests, samples of the strands from each beam were removed. An attempt was made to retrieve strands from relatively undamaged sections of the beams. The samples were tested following the procedure in ASTM A1061 (2009). Because the failure of the strand needed to be away from the gripping location, special efforts were made to cushion the gripping areas on both ends of the samples to prevent stress concentrations and premature failure. Thus, thin walled aluminum pipes were cut to 8-in lengths and then cut in half in the long direction. Each half was coated in a mixture of high-strength epoxy and grit of equal amounts, and then pressed onto the ends of the strands.

The specimens were tested in a 300-kip capacity Satec Universal Test Machine (UTM). A 9-in gage length clip-on extensometer was then attached to the strand. The load was increased at a rate of 0.025 in per second until the strand ruptured.

Analysis of Data and Development of Method for Residual Strength Calculation

For each beam tested, the first cracking load and the ultimate strength were calculated based on the material properties determined from the destructive tests and assumptions about the condition of the strands based on pre-test visual inspections and recommendations from Naito et al. (2010). The strength calculations were performed using both the strain compatibility approach and the simplified method from the LRFD Bridge Design Specifications.

In their report, Naito et al. (2010) presented an approach for assessing the reinforcement in corrosion damaged box beams. Their recommendations were as follows:

> FOR SPECIMENS WITH LONGITUDINAL CRACKING:
>
> 1. The following strand areas shall be reduced to 75% of the original cross-sectional area for capacity calculations:
>   a. Strands on each level directly in line with the crack.
>   b. Strands closest to the exterior surface adjacent to the longitudinal crack. If the adjacent strand is greater than 3 in from the crack, see the following item 2 for area reduction.
> 2. For beams with longitudinal cracking or corrosion induced spalling, all other strands in the section shall be reduced to 95% of the original cross-sectional area for capacity calculations.
>
> FOR SPECIMENS WITH DETERIORATED CONCRETE
>
> *(Adopted from "Guidelines for Estimating Strand Loss in Structural Analysis of PPC Deck Beam Bridges" by the Illinois Department of Transportation)*
>
> 1. For exposed strands observed with sound concrete adjacent to and above the exposed strands, disregard the full strength of the exposed strands for capacity calculations.
> 2. For exposed strands observed with adjacent unsound concrete, disregard the full strength of the exposed strands and all strands in regions of unsound concrete for capacity calculations.
> 3. For exposed shear reinforcement bars, disregard the full strength of strands located in the lower row directly above the exposed section of stirrups for capacity calculations. If the concrete is found to be unsound adjacent to the exposed area, disregard the strength of all strands in all rows above the area of unsound concrete in capacity calculations.
> 4. For area of concrete where delaminations have been observed, remove all delaminated concrete to determine the depth of the concrete deterioration:
>   a. If shear reinforcement bars or strands are exposed, treat as in cases "1" through "3" as shown above.
>   b. If no shear reinforcement bars of strands are exposed, but there are indications that the exposed concrete is unsound within the affected area, disregard the strength of all strands located in the rows of strands above the area for capacity calculations.
>   c. If no steel reinforcement is exposed in the affected area and the concrete is deemed as sound, do not disregard the strength of strands in the strength analysis.
> 5. For wet or stained areas of concrete observed on the bottom or the side of beams, closely inspect those areas to determine the soundness of the concrete:
>   a. If close inspection indicates that the concrete is unsound or delaminated, treat as in case "4" above.
>   b. If close inspection confirms that the concrete is sound, do not disregard the strength of strands in the strength analysis.

This method was used for assessing the condition of the reinforcement in each beam (I-Beams and Box-Beams) in this current study, and results were compared to test results in the following section.

Given the assumed condition of the reinforcement, the strength estimations were performed using a strain compatibility analysis in an Excel spreadsheet. All longitudinal steel,

both prestressed and non-prestressed, was accounted for in the analysis. In addition, the predicted strength of each beam was calculated using the simplified analysis presented in the AASHTO LRFD Bridge Design Specifications (AASHTO, 2014). Figure 23 shows the cross-section of the Lesner Bridge I-beams and Figure 24 shows the cross-section of the Aden Road Bridge box beams.

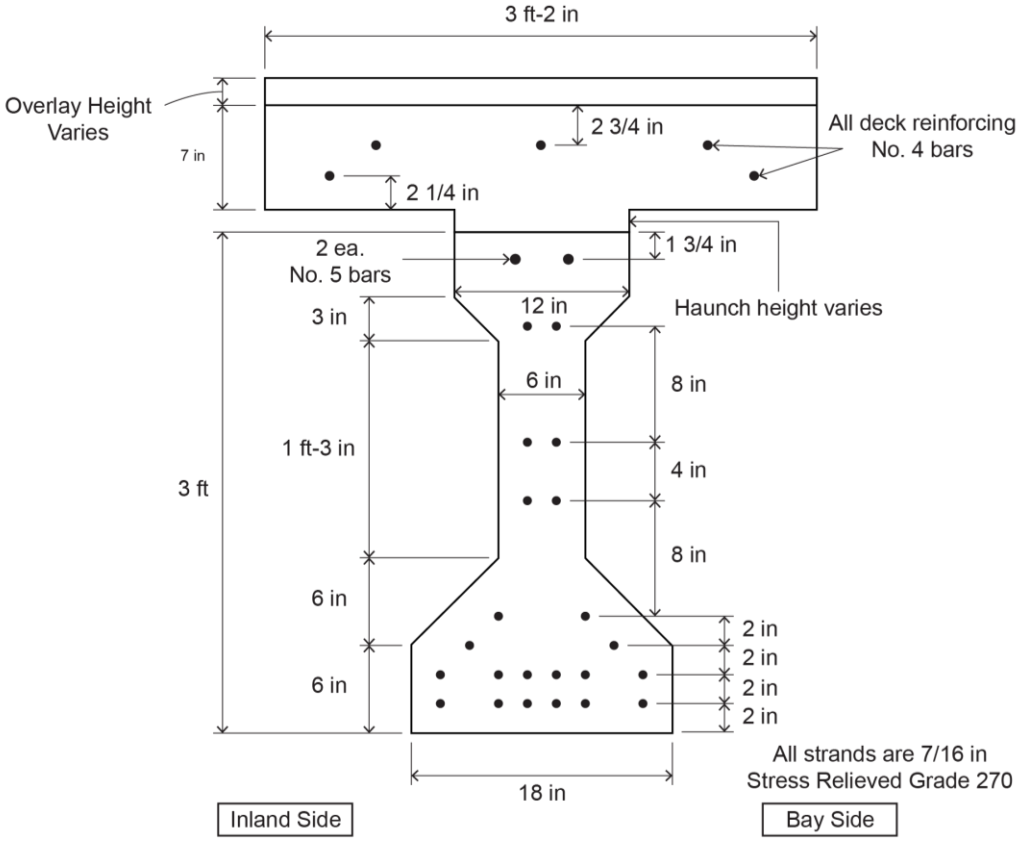

Figure 23. Cross-section of Lesner Bridge I-Beams

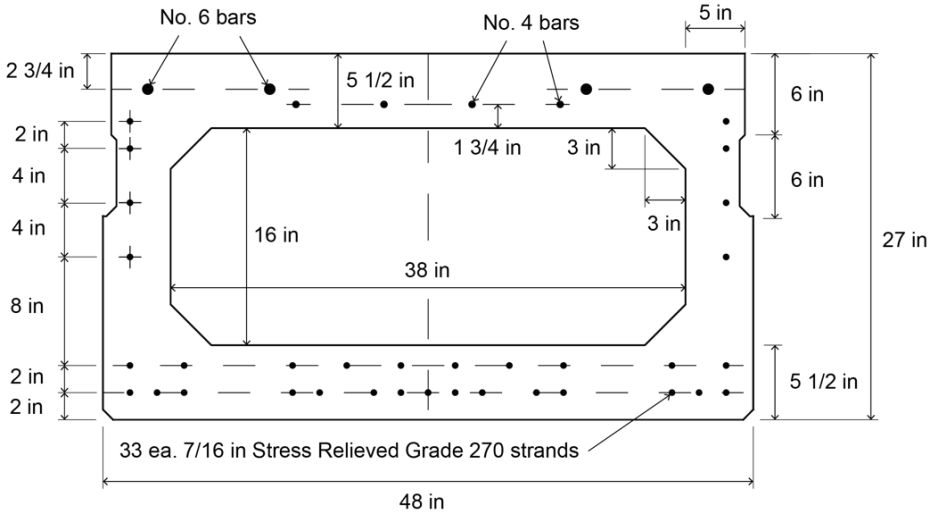

Figure 24. Cross-Section of Aden Road Bridge box beams

Finally, the researchers compared the tested strengths to the various calculations to make new recommendations for relating visible damage to prestressing strand to the reinforcement's contribution to flexural strength of prestressed beams.

RESULTS

Visual Inspection, Damage Mapping and Beam Selection

All detailed damage assessments and calculations of the damage score for each I-beam are presented in Appendix A, and final scores are shown in Table 3. Table 4 shows the score of each box beam to categorize it based on the damage factors.

Table 3. Final Damage Rating for Lesner Bridge I-Beams

Girder #	Total Long. Cracking Score	Total Amount of Section Loss Score	Total Amount of Delaminated Area Score	Total Amount of Patched Area Score	Overall Score
I-Beam 1	17.1	6.4	15.8	9.0	48.3
I-Beam 2	26.1	29.3	20.0	7.5	82.9
I-Beam 3	9.2	0.0	8.1	15.0	32.3
I-Beam 4	18.2	9.3	16.9	6.8	51.1
I-Beam 5	0.0	19.3	0.0	15.0	34.3
I-Beam 6	15.2	26.4	19.2	0.0	60.9
I-Beam 7	30.0	35.0	20.0	15.0	100.0
I-Beam 8	30.0	22.9	20.0	8.3	81.1
I-Beam 9	10.8	23.6	8.6	15.0	58.0

Note: A high score indicated good relative condition, a low score indicates poor relative condition

Table 4. Final Damage Rating for Aden Road Bridge Box Beams

Girder #	Total Longitudinal Cracking Score	Total Amount of Section Loss Score	Total Amount of Delaminated Area Score	Total Amount of Patched Area Score	Overall Score
Box-Beam 1	18.0	33.9	0.0	0.0	52.0
Box-Beam 2	21.1	0.0	0.0	0.0	21.1
Box-Beam 4	0.0	33.9	0.0	0.0	33.9

Note: A high score indicated good relative condition, a low score indicates poor relative condition

For the rating system devised, a high score indicated good condition, while a low score indicated bad condition. Based on the results presented, I-Beams 3, 6 and 7 were chosen from the Lesner Bridge. I-Beam 7 was chosen since it had the best score and would represent the baseline, undamaged state (good). I-Beam 3 was chosen since it had the worst score and would represent a severely damaged beam (bad). Finally, I-Beam 6 was chosen as an average score, representing a moderately damaged beam (medium). Of the six Aden Road box beams available, three were selected for testing. The Aden Road Bridge beams were not as accessible for inspection as the Lesner I-beams. The three beams that were most easily accessed in the storage yard were retrieved and moved into the lab. The conditions of these beams were examined once they were brought inside the testing facility. Damage maps of the six selected beams selected for study testing in this study are shown in Figures 25 through 30.

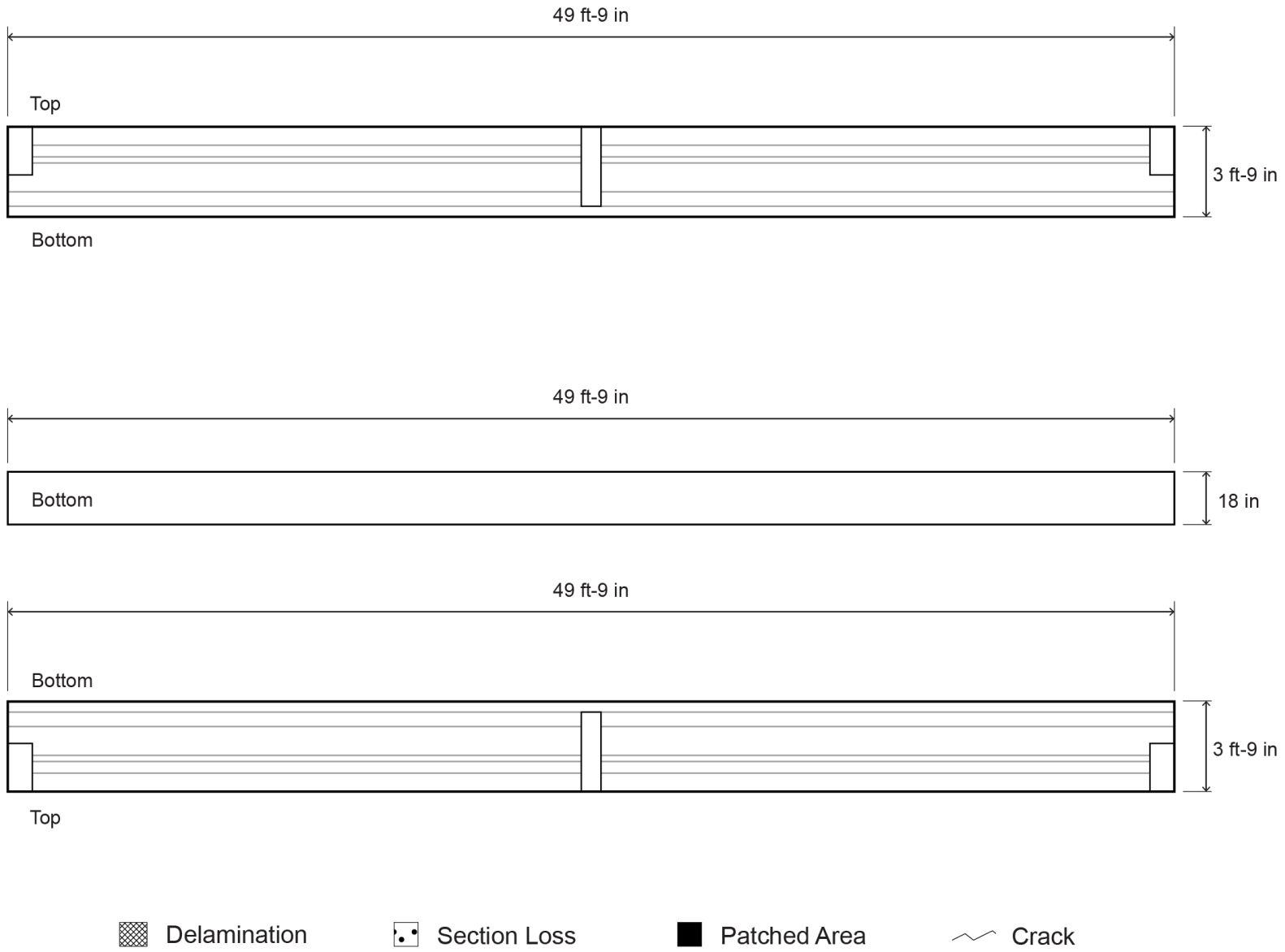

Figure 25. I-Beam 7 – Good Condition

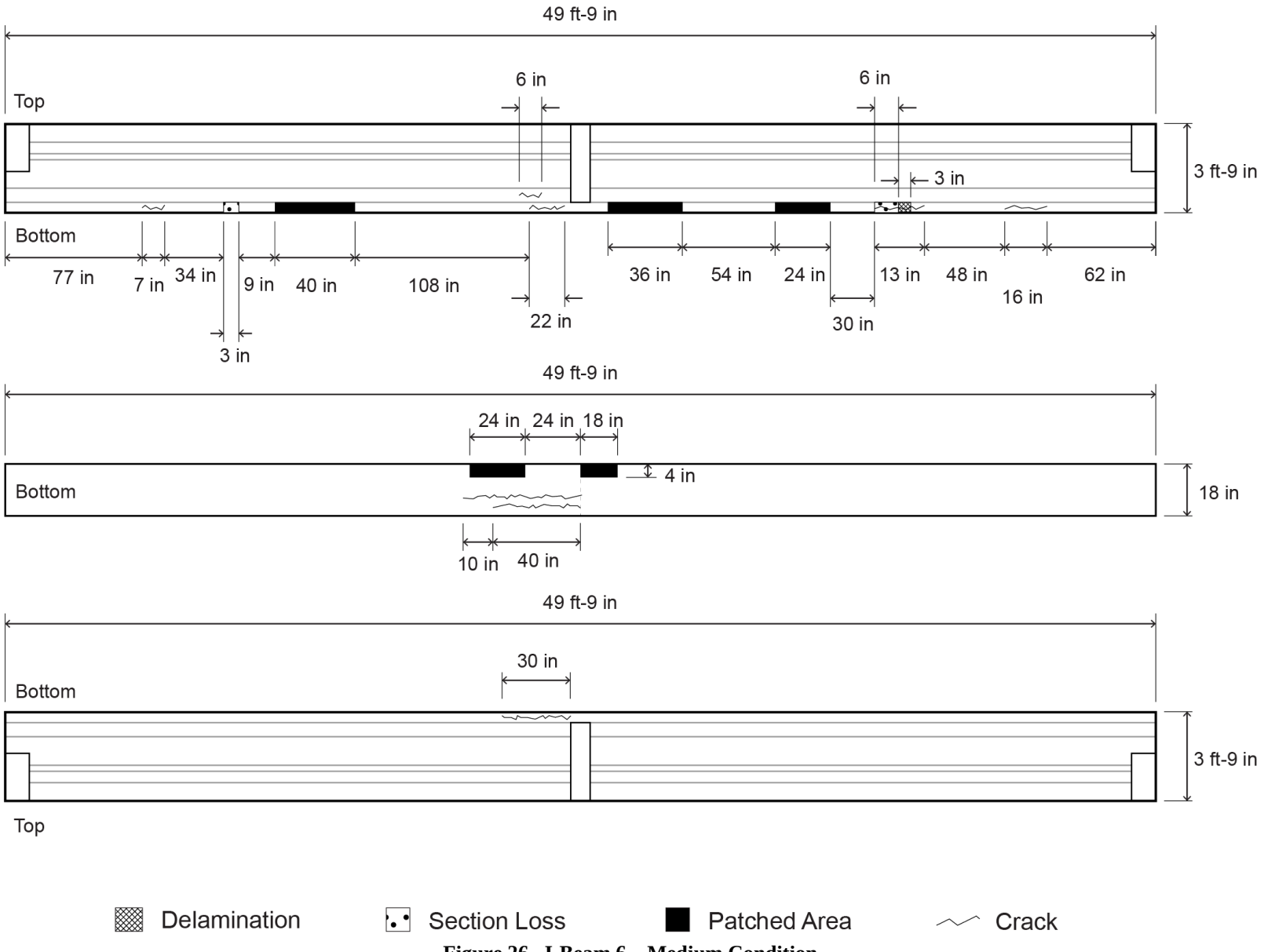

Figure 26. I-Beam 6 – Medium Condition

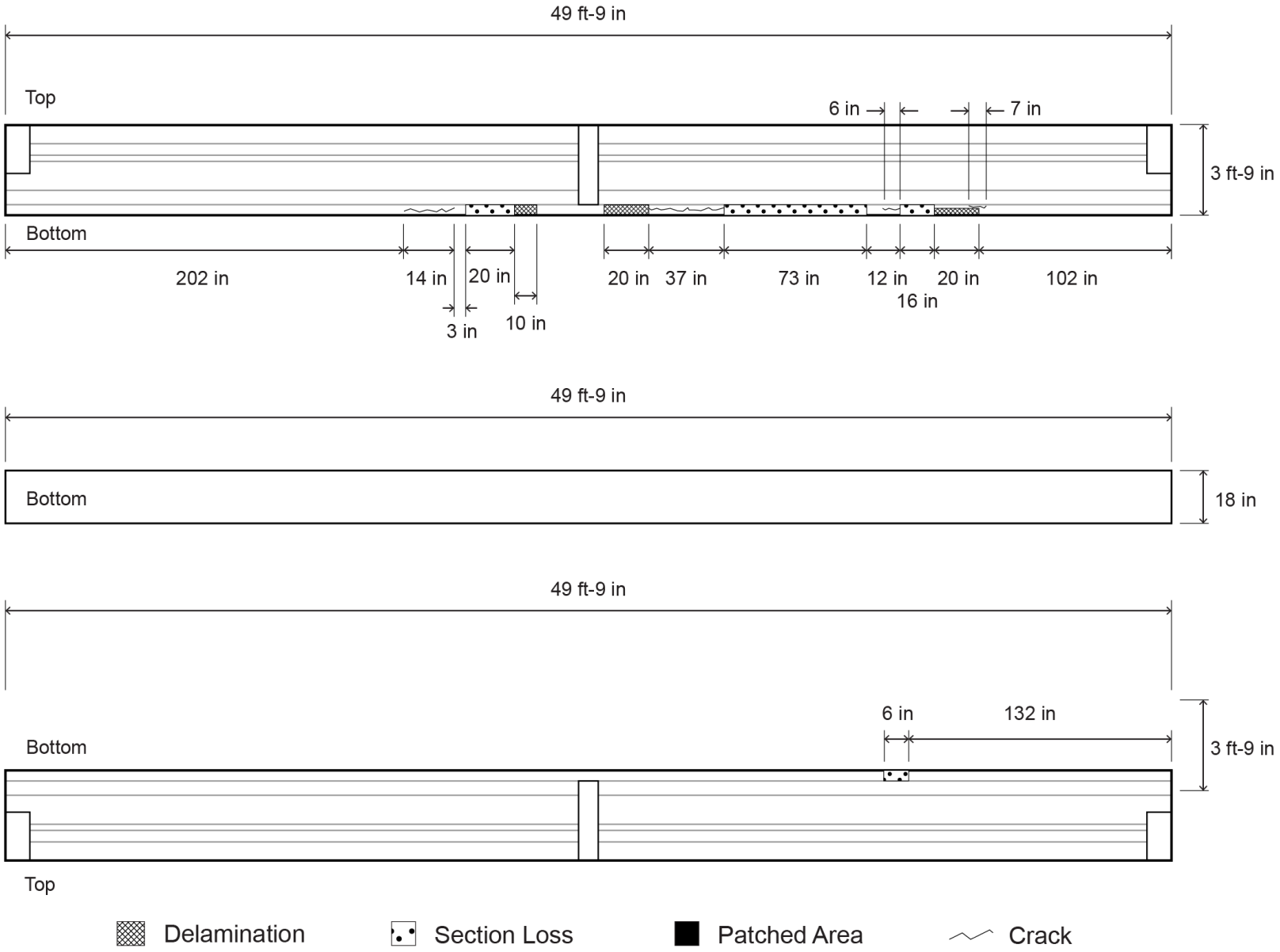

Figure 27. I-Beam 3 – Bad Condition

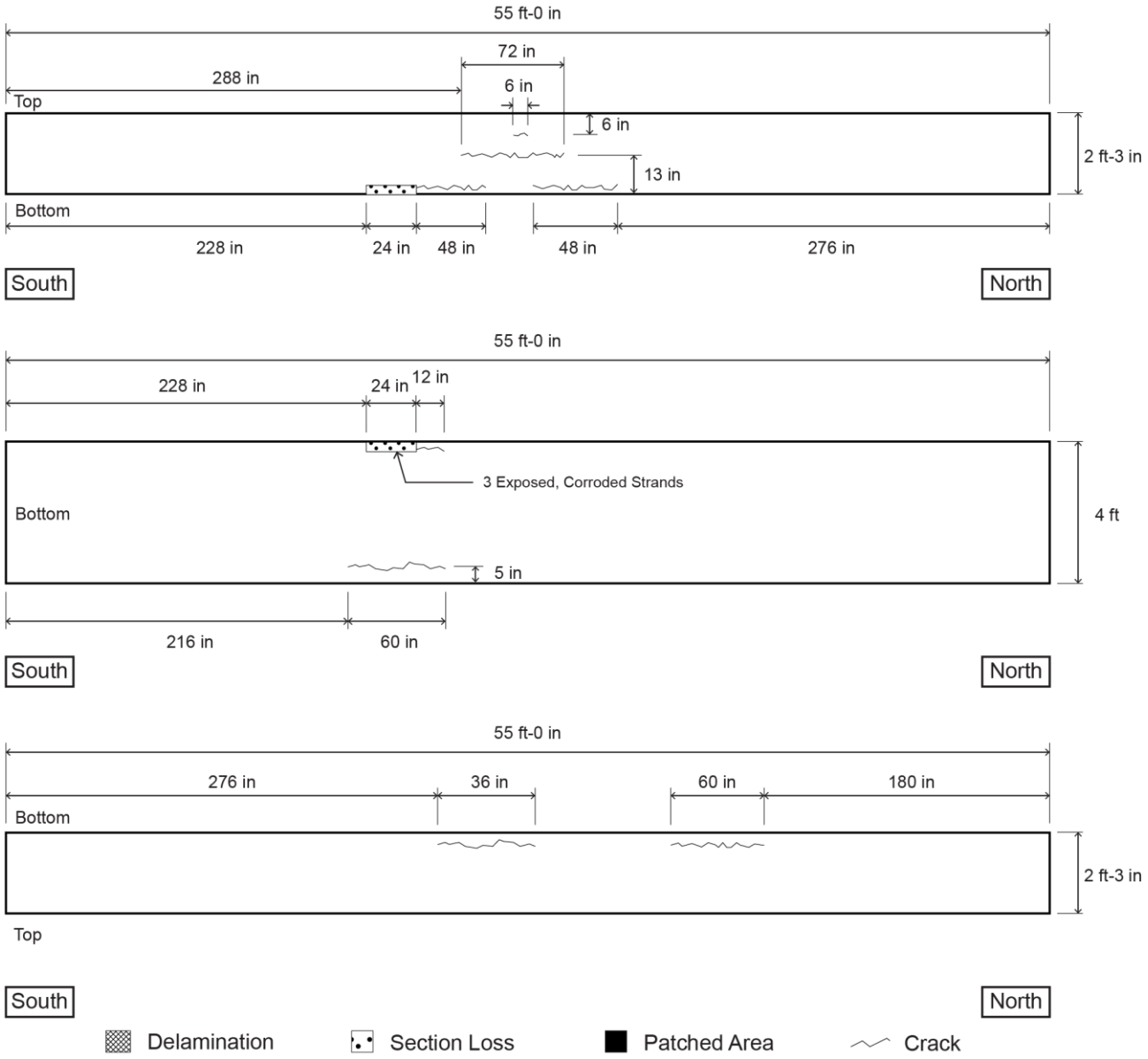

Figure 28. Box Beam 1 – Good Condition

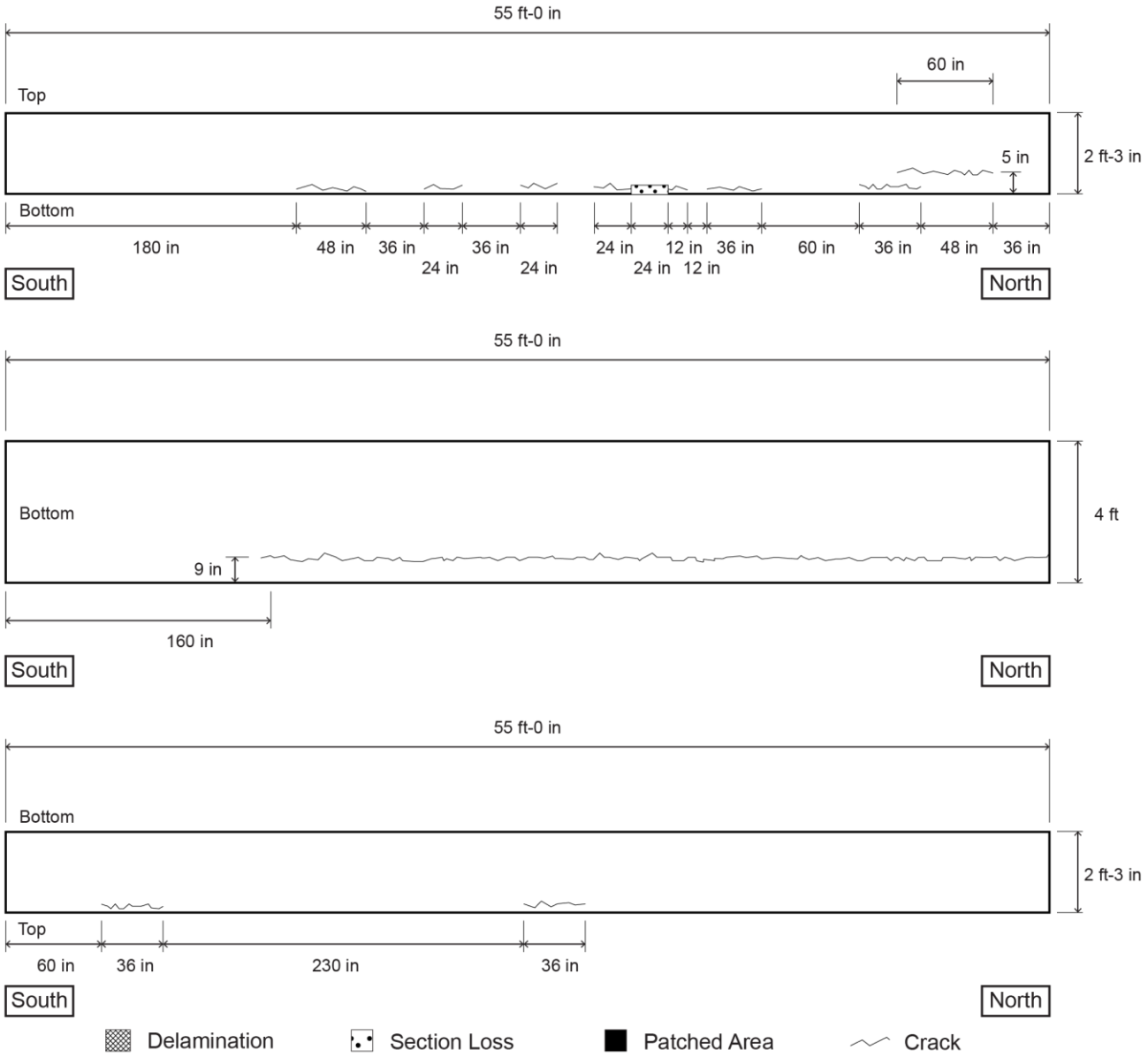

Figure 29. Box Beam 4 – Medium Condition

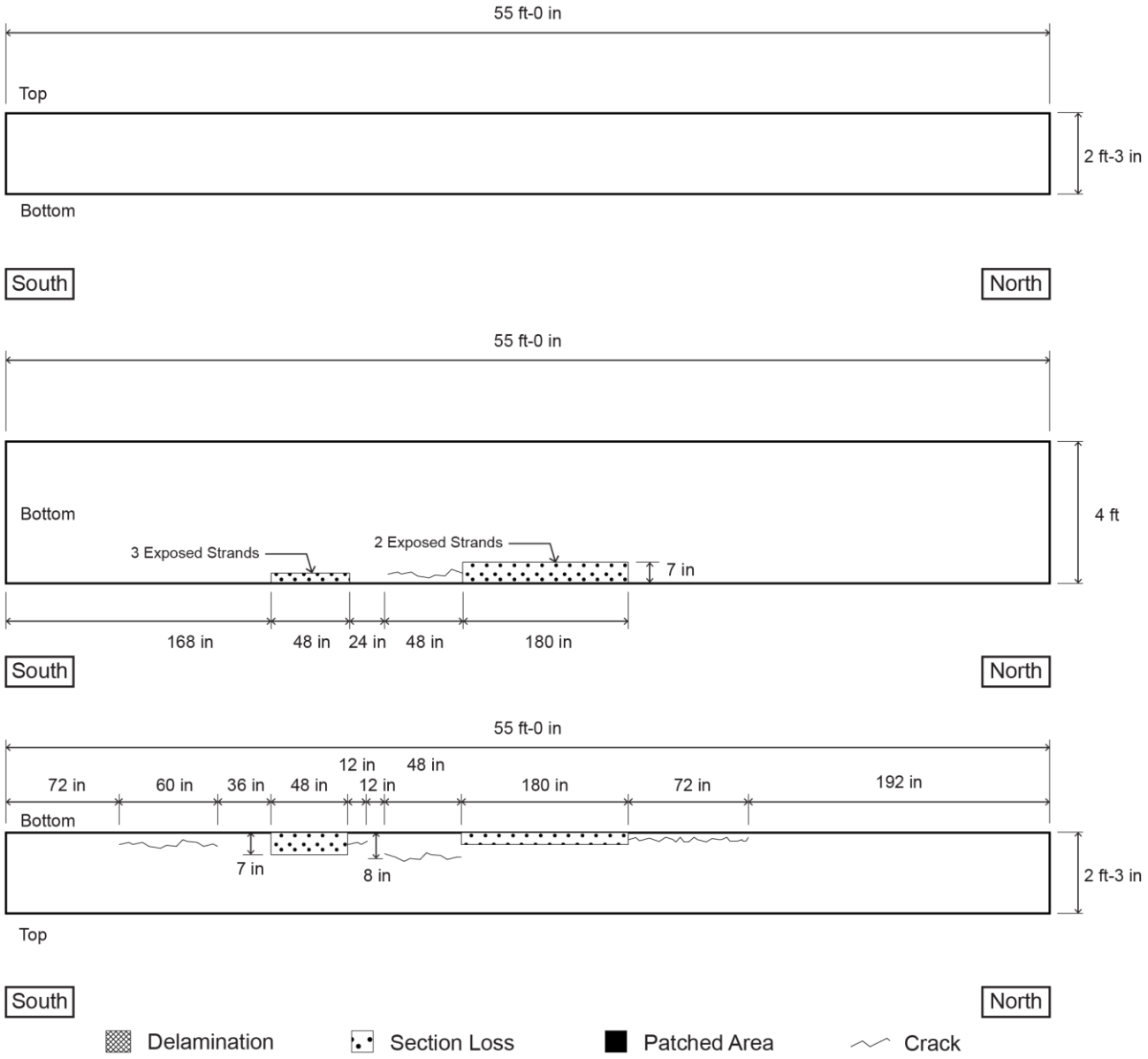

Figure 30. Box Beam 2 – Bad Condition

In Figures 25 through 30, each figure presents three sides of the beams. The top sketch is one side, oriented right-side-up, the middle sketch is the bottom of the beam, and the bottom sketch is the other side of the beam, oriented up-side-down. This allows the reader to see how side damage and bottom face damage are related to each other spatially.

Non-Destructive Evaluations

Concrete Resistivity Test

Testing was performed to determine the concrete resistivity. The results for both sides are shown in Tables 5 and 6 and Figures 31 and 32.

Table 5. Resistivity Testing – Inland Side – I-Beam 7

Measurements kΩ.cm	Area %	Risk of Corrosion
(<10)	0%	High
(10 to 50)	17%	Medium
(50 to 100)	2%	Low
(>100)	81%	Negligible

Table 6. Resistivity Testing – Bay Side – I-Beam 7

Measurements kΩ.cm	Area %	Risk of Corrosion
(<10)	0%	High
(10 to 50)	15%	Medium
(50 to 100)	4%	Low
(>100)	80%	Negligible

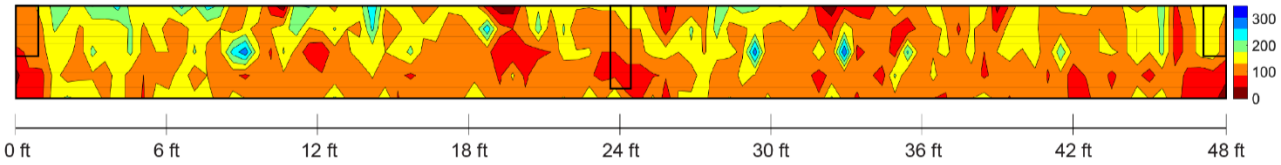

Figure 31. Inland Side of I-Beam 7 Resistivity Reults (kΩ.cm)

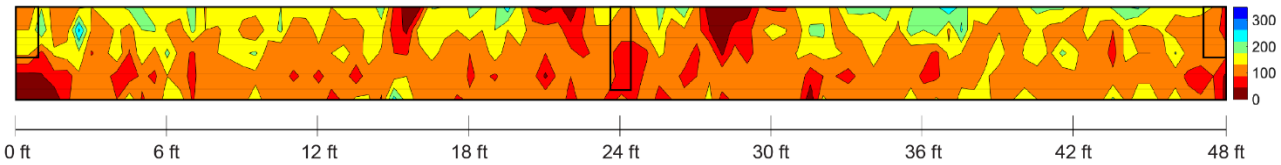

Figure 32. Bay Side of I-Beam 7 Resistivity Results (kΩ.cm)

According to the results for I-Beam 7, the risk of corrosion was very low. It was hypothesized that one of the reasons why the resistivity measurements were so low was that the beams were very dry. This prevented the electric current from passing through the concrete, which resulted in very low readings. Based on the poor results of this test, and the fact that all other beams were expected to be in similar dry conditions, the concrete resistivity test was not performed for the other beams. It would have been possible to wet down the beams to improve

the results of the resistivity testing, but since this would most likely not be an option in actual field situations, wetting was not performed.

Half-Cell Potential Test

As discussed in the Methods section, half-cell corrosion mapping was used to identify the possibility of active corrosion in the girders. Unfortunately, for I-Beam 3, which was in poor condition, the half-cell potential data could not be retrieved from stored files, and no back-ups had been made. For the good condition I-Beam 7, the half-cell did not show any indication of corrosion, which matched the visual damage maps. For I-Beam 6, which was considered to be in medium condition, visual inspections indicated active corrosion along much of the bottom flange of the bay side of the beam. The half-cell also indicated possible corrosion along the bay side bottom flange and near the ends of the beam.

All of the Aden Road box beams showed high potential for corrosion along the bottom edge of the beams. These results for the box beams are in agreement with the visual inspection, which indicated considerable spalling, delamination and exposed, corroded strands.

The available results of the corrosion potential for the girders are shown in Figures 33 through 42. In all figures, blue indicates a low probability of active corrosion, and dark red indicates a high probability.

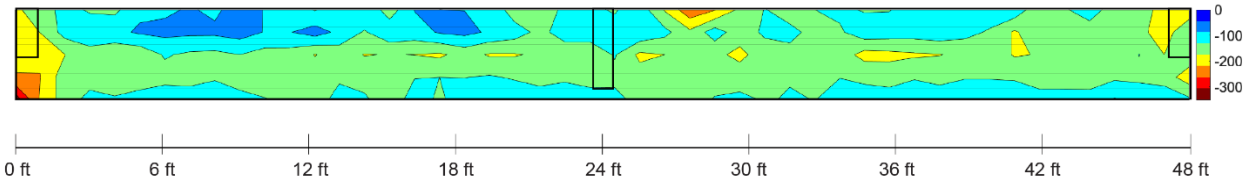

Figure 33. Half-Cell Potential Results for I-Beam 7 - Good Condition - Bay Side (mV)

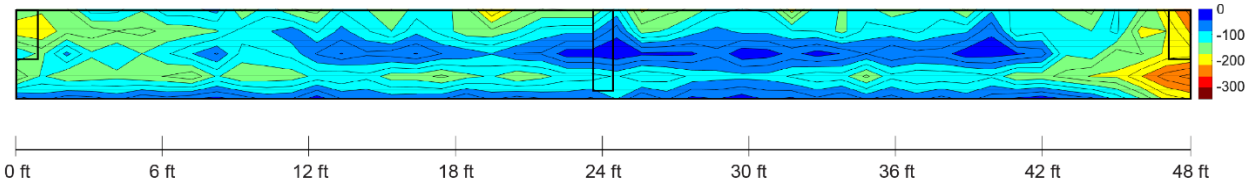

Figure 34. Half-Cell Potential Results for I-Beam 7 - Good Condition - Inland Side (mV)

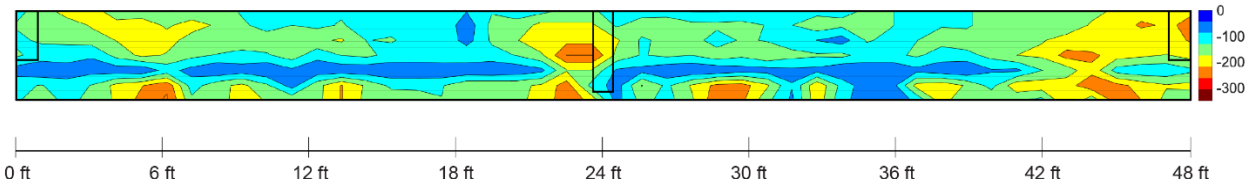

Figure 35. Half-Cell Potential Results for I-Beam 6 - Medium Condition - Bay Side (mV)

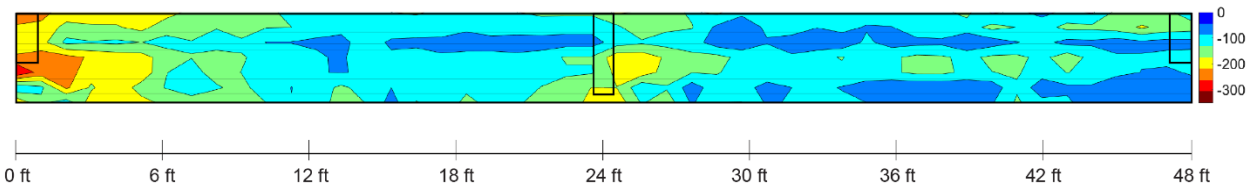

Figure 36. Half-Cell Potential Results for I-Beam 6 - Medium Condition - Inland Side (mV)

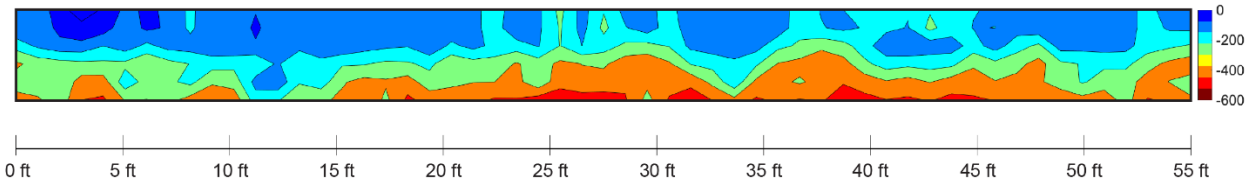

Figure 37 Half-Cell Potential Results for Box Beam 1 – Good Condition - East Side (mV)

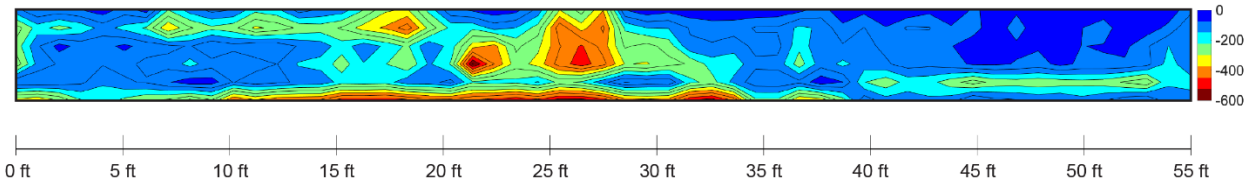

Figure 38. Half-Cell Potential Results for Box Beam 1 - Good Condition - West Side (mV)

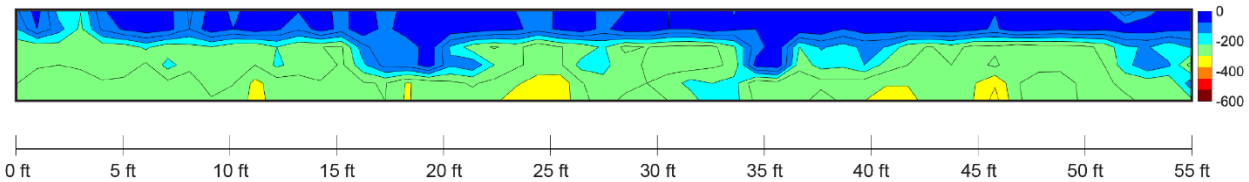

Figure 39. Half-Cell Potential Results for Box Beam 4 – Medium Condition - East Side (mV)

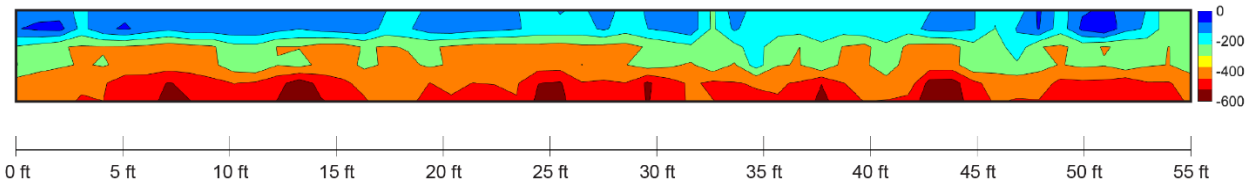

Figure 40. Half-Cell Potential Results for Box Beam 4 – Medium Condition - West Side (mV)

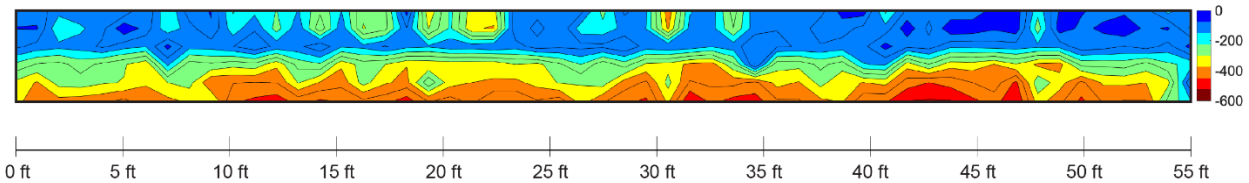

Figure 41. Half-Cell Potential Results for Box Beam 2 – Bad Condition - East Side (mV)

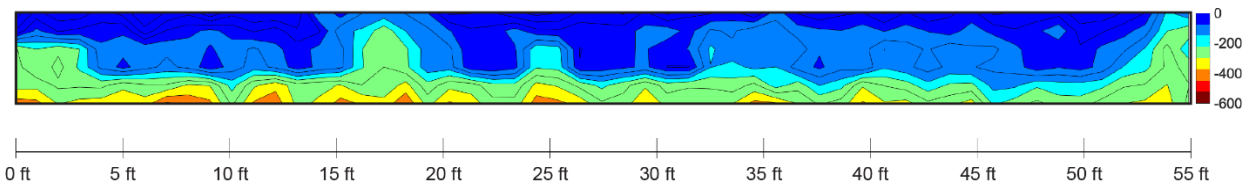

Figure 42. Half-Cell Potential Results for Box Beam 2 – Bad Condition - West Side (mV)

Tests to Determine Flexural Strength

I-Beam 7 – Good Condition

I-beam 7 represented an undamaged control test to provide a baseline for comparison with subsequent tests. The beam was tested over two days; on the first day, a load of 179 kips

was applied in increments and the measured deflection was 6.87 in. Cracks were first observed at 85 kips. After a load of 105 kips, the beam was no longer closely inspected between load intervals, for safety purposes. At a load of 179 kips, an unexpected inclination of the actuator was observed, so the test had to be stopped until the issue could be fixed.

One week later, the beam was re-tested. The load was applied in increments of 20 kips until reaching 140 kips, at which point 10-kip increments were applied until the failure load of 190 kips with a deflection of 8.93 in. The failure was caused by crushing of the top slab as shown in Figure 43. The beam after testing is shown in Figure 44.

Figure 43. Crushing Failure in Top Slab of I-Beam 7

Figure 44. Residual Deflection after Testing I-Beam 7

The load-deflection plot is shown in Figure 45 for first day and second day. For the first day test, a slight change in the slope of the line can be seen at around 80 kips, confirming the

first cracking load determined visually. For the second day test, at around 190 kips the load-deflection curve begins to plateau, indicating the strands were yielding.

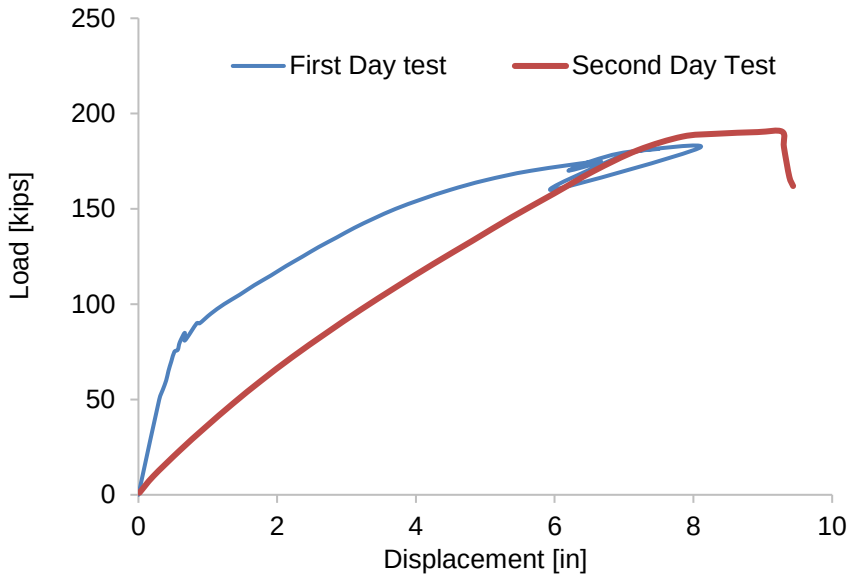

Figure 45. Load Versus Displacement on First and Second Day of Testing I-Beam 7

Figure 46 shows a plot of longitudinal strain versus distance from the bottom of the beam measured by the gages at mid-span of the beam. Several load steps are presented in the figure. The neutral axis determined from the strains measured just before the cracking load is 26 in from the bottom of the beam. The neutral axis based on calculation, including all the strands and the concrete modulus obtained from the compressive strength test, was 28.8 in, which was 10% higher than the measured neutral axis. The strain distributions were relatively linear, except for the upper most and lower most gages. However, the highest strain reading was on the side of the slab, and for unknown reasons, was larger than expected based on calculations. The strains on the bottom flange were smaller than expected, possibly due to the damage to the concrete on the bottom.

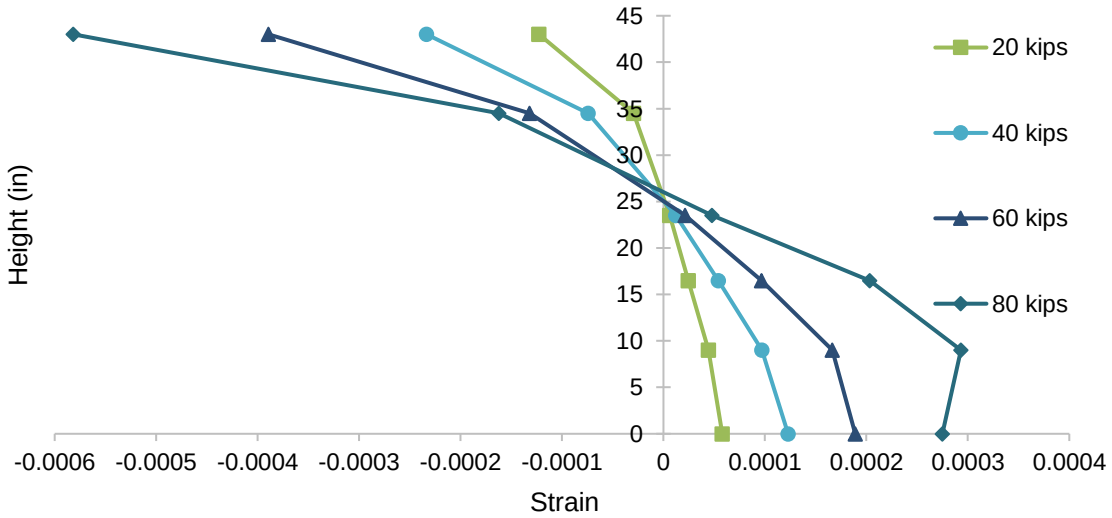

Figure 46. Strain Versus Height for I-Beam 7

After testing, the concrete cover over the bottom strands was chipped to expose the strands. As can be seen in Figure 47, all strands were bright and shiny, showing no signs of corrosion.

Figure 47. Bottom of I-Beam 7 after Testing

I-Beam 6 – Medium Condition

I-Beam 6 failed at an applied load of 118 kips and a deflection of 4.46 in, due to crushing of the top flange. The load versus deflection plot is shown in Figure 48. The first crack was visually observed at 50 kips; however, there was no noticeable change in the slope of the load displacement plot at that load.

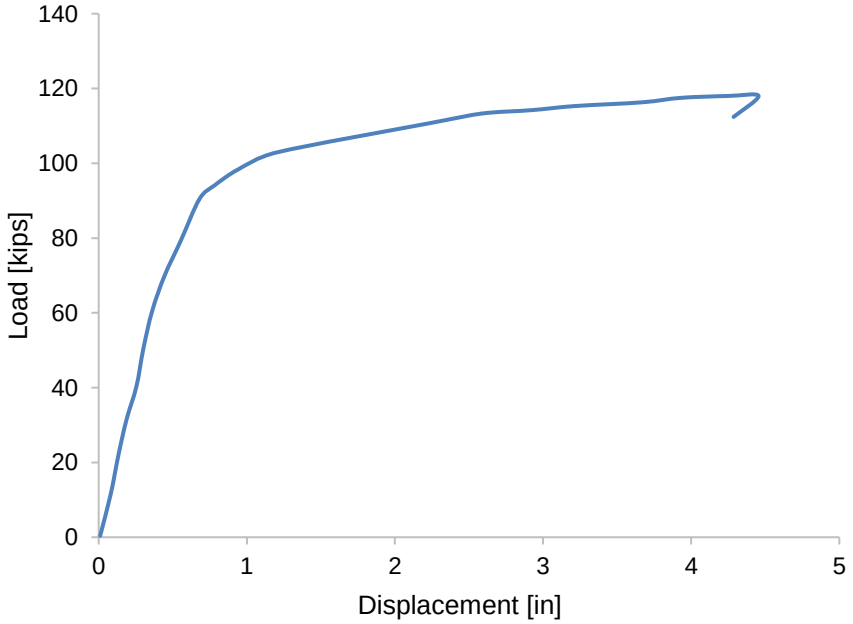

Figure 48. Load Versus Displacement Plot for I-Beam 6

Figure 49 is a plot of longitudinal strain at mid-span versus distance from the bottom of the beam for several different load steps. The figure indicates that the measured neutral axis prior to cracking was 24 in, while the calculated neutral axis was 26 in, based on the remaining cross-sectional area of the strands and the tested concrete compressive strength. The difference of the neutral axis location was about 8%. As with the strains measured for I-Beam 7, the gage on the top slab had strain readings that were higher than expected.

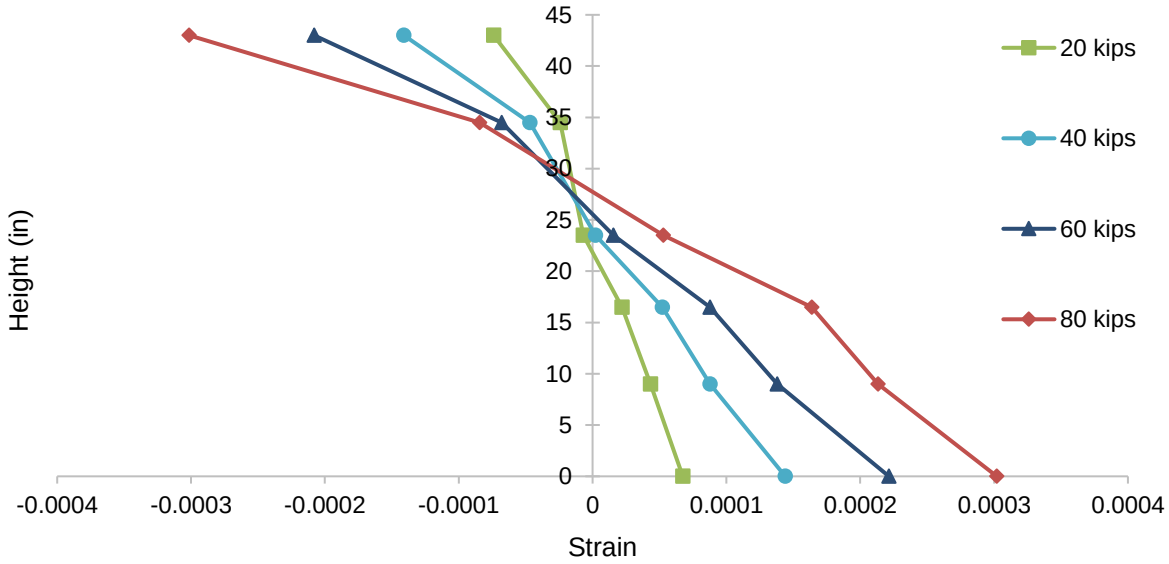

Figure 49. Strain Versus Height for I-Beam 6

This beam was considered to be in medium condition. Near the mid-span on the bay side of the bridge there was a patch on the bottom flange that extended a few feet on either side of the mid-span diaphragm of the beam. Figure 50 shows the cracking that developed along the patch during testing.

Figure 50. Cracking along Patch During Testing of I-Beam 6

The opposite side of the beam showed very little sign of corrosion damage, except for one 8-in long hairline crack 2 in up on the bottom flange. As testing progressed, a spall occurred at the crack, revealing the corroded strand beneath (see Figure 51). Also in Figure 51, rust staining can be seen on the bottom flange; a post-test autopsy confirmed that the chairs supporting the reinforcement during concrete placement were in fact corroded. This type of staining was also seen on I-Beam 7 (see Figure 47).

Figure 51. Hairline Crack Observed Prior to Testing (marked in green) Related to Corroded Strand Beneath on I-Beam 6

After testing was completed, the concrete on the bottom flange was removed to investigate the condition of the strands, as shown in Figure 52. Upon careful inspection, it was determined that five of the six bottom row strands showed signs of severe corrosion with most wires broken, apparently due to the aforementioned corrosion. A few wires appeared to have broken during testing and showed a shiny surface. Interestingly, the fourth strand, counting from the top of Figure 52, showed no evidence of corrosion damage. The bottom strand in the photo, still embedded in a piece of the patch material, showed evidence of being broken before testing, and most likely at the time the patch was applied. The strand in the same position, but in the second row, was also in the patch and was in similar condition.

Figure 52. Bottom Flange of I-Beam 6 after Testing

I -Beam 3 – Bad Condition

The first flexural crack of the I-beam in "bad condition", I-Beam 3, was observed at a load of 80 kips. For reasons of safety, the beam was no longer closely inspected between load intervals after an applied load of 125 kips. The load deflection plot is presented in Figure 53. Based on strain measurements through the depth of the beam, the neutral axis, just before the cracking load, was 26 in from the bottom of the beam (see Figure 54), which is comparable to the calculated neutral axis of 26.7 in, which was based on the cross-sectional area of the remaining strands and the concrete compressive strength from testing. The beam ultimately failed due to crushing of the top flange (see Figure 55), with an applied load of 166 kips and a deflection of 8.19 in.

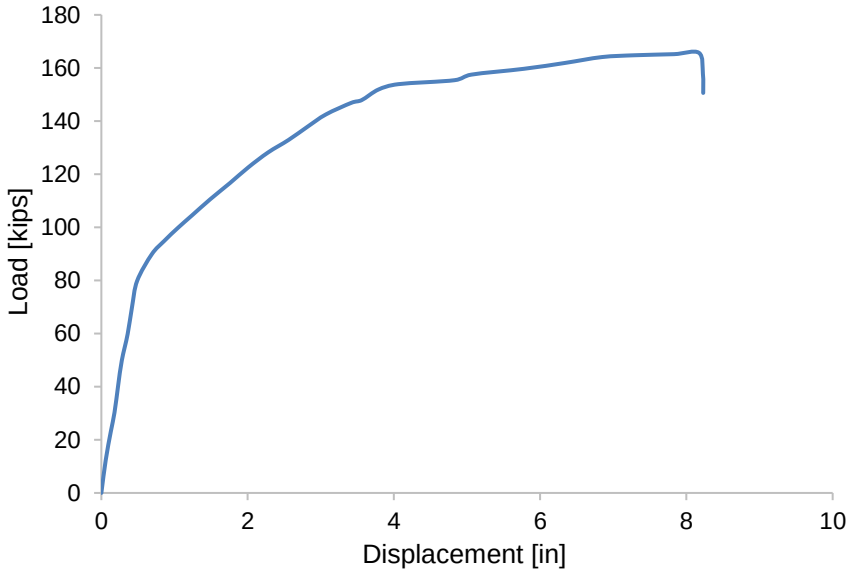

Figure 53. Load Versus Displacement Plot for I-Beam 3

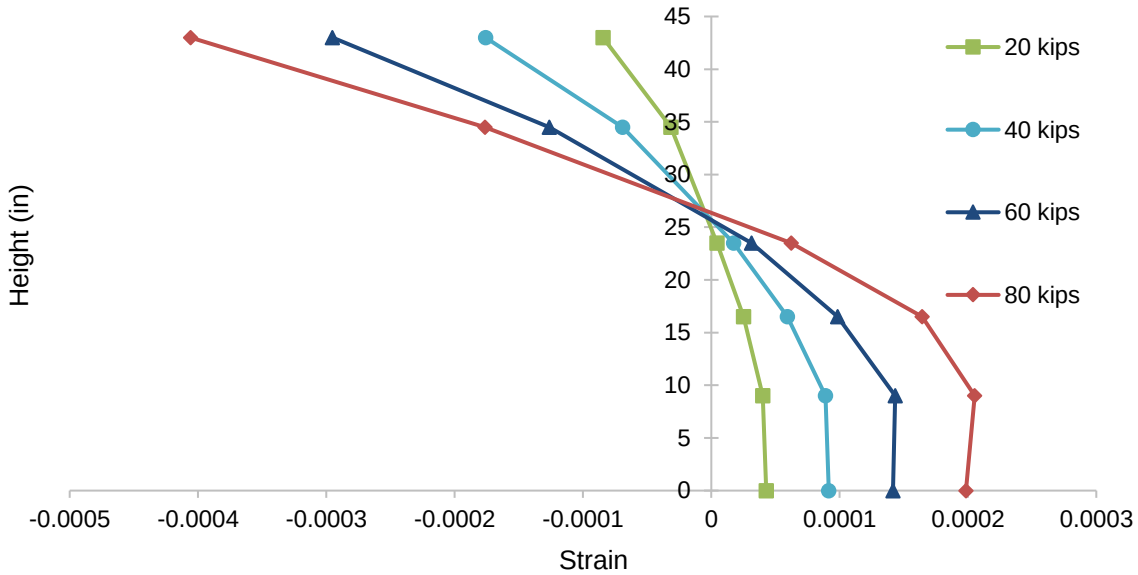

Figure 54. Strain versus Height of I-Beam 3

Figure 55. Crushing of Top Flange at Failure of I-Beam 3

This beam was considered to be in poor condition, with considerable patching and spalling all along the bay side of the bottom flange. Figure 56 shows the top flange crushing at the completion of testing, and also the bottom flange cracking associated with the corroded strands and patching.

Figure 56. I-Beam 3 after Testing

After testing, the bottom flange was examined and it was determined that the strand in the patch and the strand directly above it in the original concrete were both badly damaged and fractured from corrosion (see Figure 57). In addition, a second bottom-row strand in the patch was damaged. The remainder of the strands were in relatively undamaged condition.

Box-Beam 1 – Good Condition

First cracking was observed at a load of 50 kips. After cracking, the researchers applied additional load in 5-kip increments up to 70 kips, after which, the beam was no longer closely inspected, out of concern for safety. Also, after 70 kips, displacement control was used with 0.25-in increments. The test was terminated at 90.3 kips, when the deflection reached 16.99 in without any increase in load. This can be seen in the load versus deflection plot in Figure 58. The large deflection at the ultimate load can be seen in Figure 59.

Figure 57. Corrosion-Damaged Strands in and above Patch in I-Beam 3

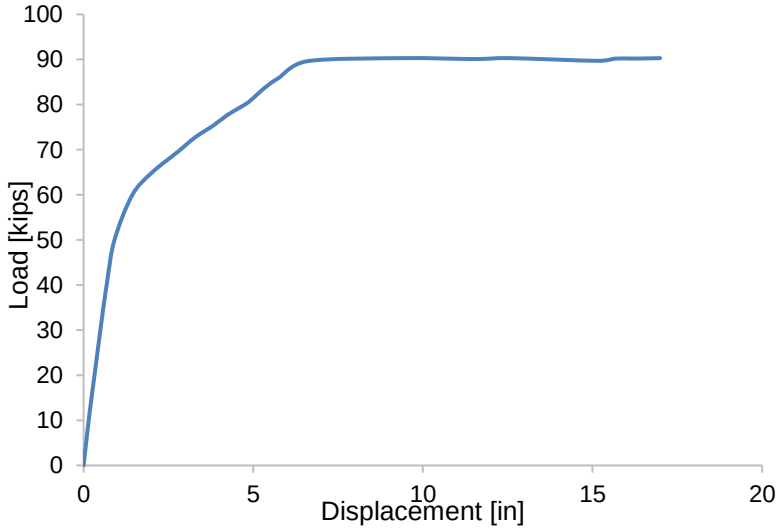

Figure 58. Load Versus Displacement Plot for Box Beam 1

Figure 59. Large Deflection of Box Beam 1

Based on the mid-span strain measurements through the depth of the beam and just before the cracking load, the neutral axis was 13.5 in from the bottom of the beam (see Figure 60). The neutral axis based on calculation was also 13.5, identical to the neutral axis determined from measurements. A slight change in the location of the neutral axis can be seen at the 50 kip load increment, which corresponds to the load at which cracking was observed. Again, the measurements from the strain gages became erratic shortly after first cracking. Thus, Figure 60 only contains data up to that point.

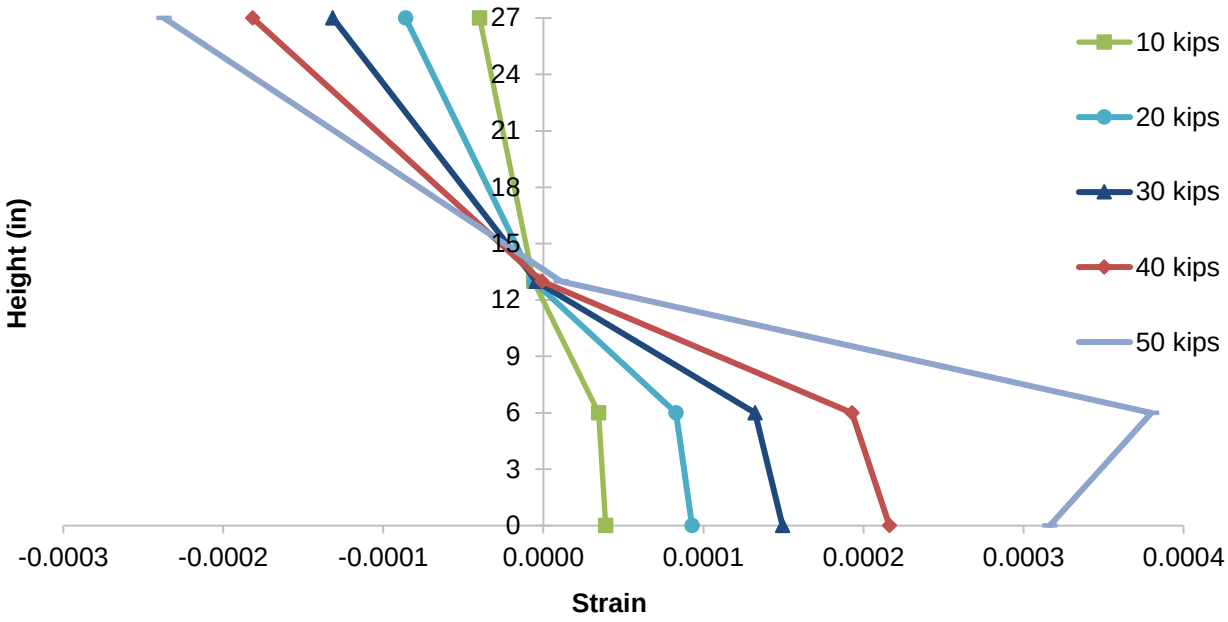

Figure 60. Strain Versus Height for Box Beam 1

Before the test, severe corrosion was observed in the three bottom strands on the west side of the beam (see Figure 61). The cracks during the test were marked and the propagation was observed (see Figure 62 and 63). Figure 64 shows the beam at the completion of testing.

Figure 61. Condition of the West Side of Box Beam 1 Before the Test

Figure 62. Condition of the East Side of Box Beam 1 Before the Test

Figure 63. Propagation of the Cracks of the East Side of Box Beam 1 During the Test

Figure 64. Condition of the East Side of Box Beam 1 at the End of the Test

Box-Beam 4 – Medium Condition

First cracking was visually observed at a load of 45 kips, as confirmed by the change in slope of the load-deflection plot in Figure 65. During the test and at high deflection, considerable water began leaking from the void in the beam. At that point, the load was held constant, and buckets were used to collect the leaking water. After a load of 65 kips, the beam was no longer closely inspected, due to safety concerns. The beam failed when the corroded strands ruptured at an applied load of 83.8 kips. Unfortunately, there was some difficulty with the data collection system before approximately 52 kips of applied load. Thus, strain measurements were not recorded. Additionally, deflection readings were taken manually after 52 kips of applied load, thus the deflection data in the second part of the test was not as accurate as in the previous tests.

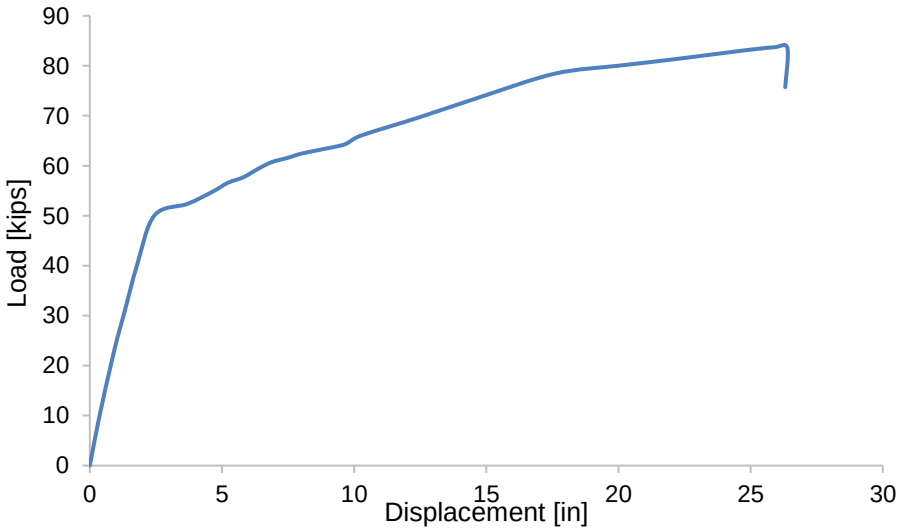

Figure 65. Load Versus Displacement Plot for Box Beam 4

Figure 66 shows a horizontal crack along the east side of the beam prior to testing. Upon examination after the test, strands along that side did not show significant corrosion, but the strands had yielded (see Figure 67). Figure 68 shows the condition of the west side before testing. It can be seen that the edge strands in the lowest level had severe corrosion, possibly exacerbated by the water that had been trapped in the beam. Figure 69 and Figure 70 show the condition of the west side of the box beam after testing. After the bottom concrete cover had spalled off, it was apparent that the three outermost bottom layer strands were severely corroded.

Box-Beam 2 – Bad Condition

Cracking in the concrete was first visually observed at a load of 49 kips, and signs of yielding occurred at 65 kips. At that point, subsequent loading was displacement-controlled (in 0.5-in increments) until the load reached 80 kips. After 80 kips, the beam was deflected in 0.25-in increments until failure, which was crushing in the top concrete at an applied load of 91.6 kips and a deflection of 17.2 in. Note that the test was stopped, unloaded and reloaded twice at 90 kips due to reaching the maximum extension of the piston in the actuator. Also note that, for

Figure 66. Box Beam 4 East Side Before Testing

Figure 67. Box Beam 4 East Side after Testing

Figure 68. Box Beam 4 West Side Before Testing

Figure 69. Box Beam 4 West Side After Testing

Figure 70. Strand Condition for Box Beam 4 West Side

safety purposes, the beam was no longer closely inspected after 65 kips of applied load. Figure 71 presents the load-versus-displacement plot, and Figure 72 shows the top flange crushing.

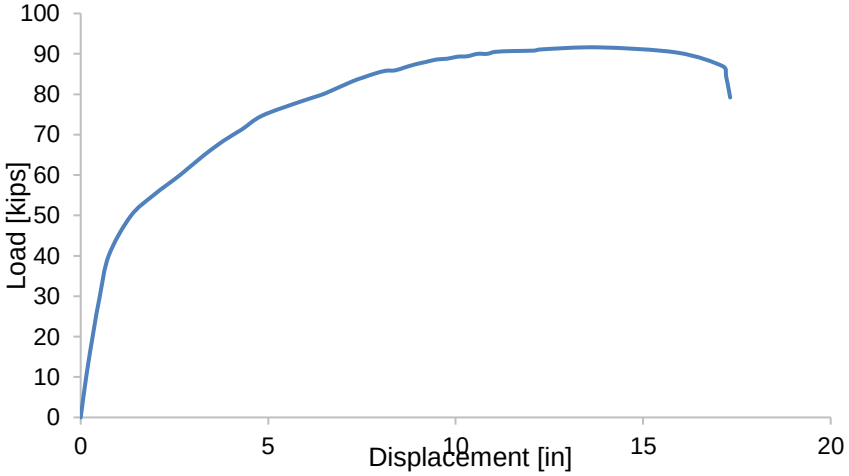

Figure 71. Load versus Displacement Plot for Box Beam 2

Figure 72. Crushing of the Top Flange of Box Beam 2

Based on strain measurements through the depth of the beam at mid-span from loads of 10 kips to 30 kips, the neutral axis was 13.5 in from the bottom of the beam (see Figure 73). The neutral axis based on calculation was also 13.5 in, identical to the neutral axis determined from measurements. Note that the height to the neutral axis increased at 40 kips, indicating that there may have been some microcracking that was not visible to the naked eye. Also note in Figure 71, the change in slope of the load-deflection plot occurred near 40 kips, which also indicated that cracking occurred before it was visually identified at 49 kips. Note that the measurements from the strain gages became erratic shortly after first cracking. Thus, Figure 73 only contains data up to that point.

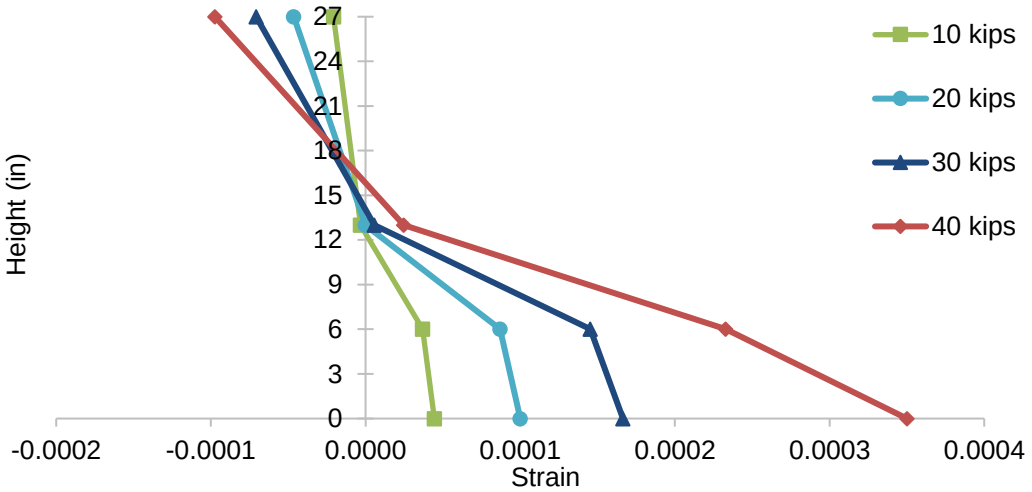

Figure 73. Mid-span Strain Versus Height of Box Beam 2

Figure 74 shows the very large deflection in the beam during the test. Figure 75 shows the severely corroded lower strand in the east side, which was observed before the test. After testing, the researchers found that the other strands were relatively undamaged.

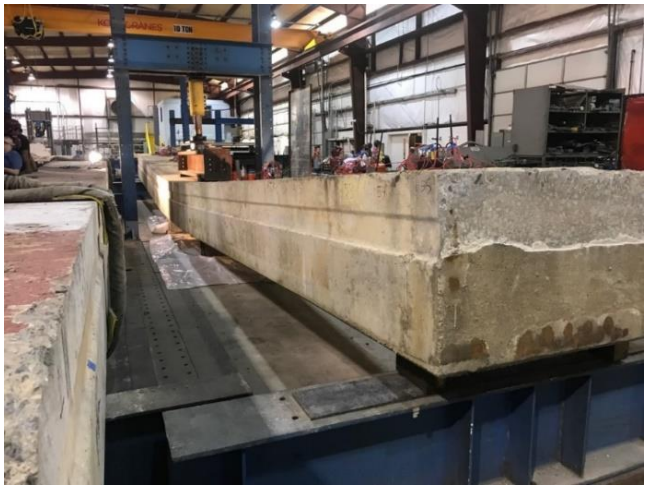

Figure 74. Large Displacement of Box Beam 2

Figure 75. Corroded Strand on Bottom of Box Beam 2

Post-Test Destructive Testing

Total Chloride Evaluation

This section presents the results of the chloride concentration tests on powdered samples obtained from the tested beams. For comparison to the test results, the criteria for corrosion risk compared to chloride content in Europe are given in Table 7 (Broomfield, J.P, 2007)

Table 7. Risk of Corrosion Compared to Chloride Content

% Chloride by mass of sample (concrete)	Risk	Chloride content per volume of concrete (lb/yd^3)
<0.03	Negligible	<1.17
0.03-0.06	Low	1.17-2.35
0.06-0.14	Medium	2.35-5.48
>0.14	High	>5.48

I-Beam 7 - Good Condition

The results of chloride content testing for I-Beam 7 are shown in in Figure 76. Figure 11 shows the locations of the extracted samples on I-Beam 7, with "Horizontal" on the chart referring to the sample taken from the side of the bottom flange, and "Inclined" referring to the samples taken from the inclined face of the bottom flange.

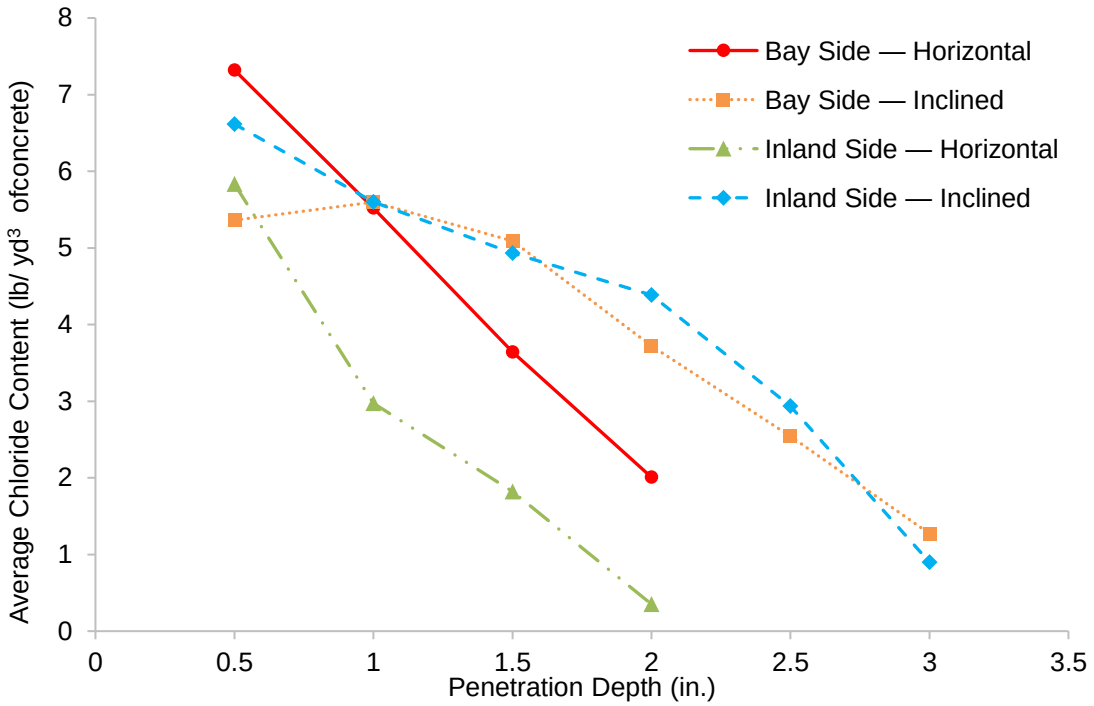

Figure 76. Results of Chloride Testing for I-Beam 7

For I-Beam 7, the chloride concentration of all of the sides decreased significantly as the depth of the sample increased. The only exception was the bay side – inclined which had a slight increase in the chloride content from 0.5 in to 1.0 in. For the samples taken from the vertical faces, the chloride content in the bay side was substantially higher than the inland side at each depth point, likely because the bay side was exposed to a harsher environment compared to the inland side. On the inclined faces, the bay and inland sides had very similar chloride contents at each depth, and were higher than the vertical faces. This could be explained by salts being deposited on the inclined faces, and not washing away as easily as on the vertical faces.

I-Beam 6 – Medium Condition

The results of chloride content testing for I-Beam 6 are shown in Figure 77. Figure 12 shows the locations of the extracted samples on I-Beam 6. The bay side – horizontal sample had a steep increase in the chloride content from 0.5 in to 1.0 in; this result can be explained by the fact that water or rain could probably wash off chloride content at the concrete surface which resulted in a low reading. The inland side – horizontal showed similar results as the bay side – horizontal, but with slightly lower chloride concentrations. This result can be explained by the fact that the bay side was subjected to higher chloride exposure as the wind coming from the bay

side direction pushed salt directly onto the bay side surface of the beams. For both sides, the chloride content in the inclined face of the bottom flange in the girder decreased considerably from 1.0 in to 3.0 in. with the inland side, surprisingly, having a higher chloride content. It is not known why the chloride concentration on the inland side is higher, as it is subjected to a milder environment.

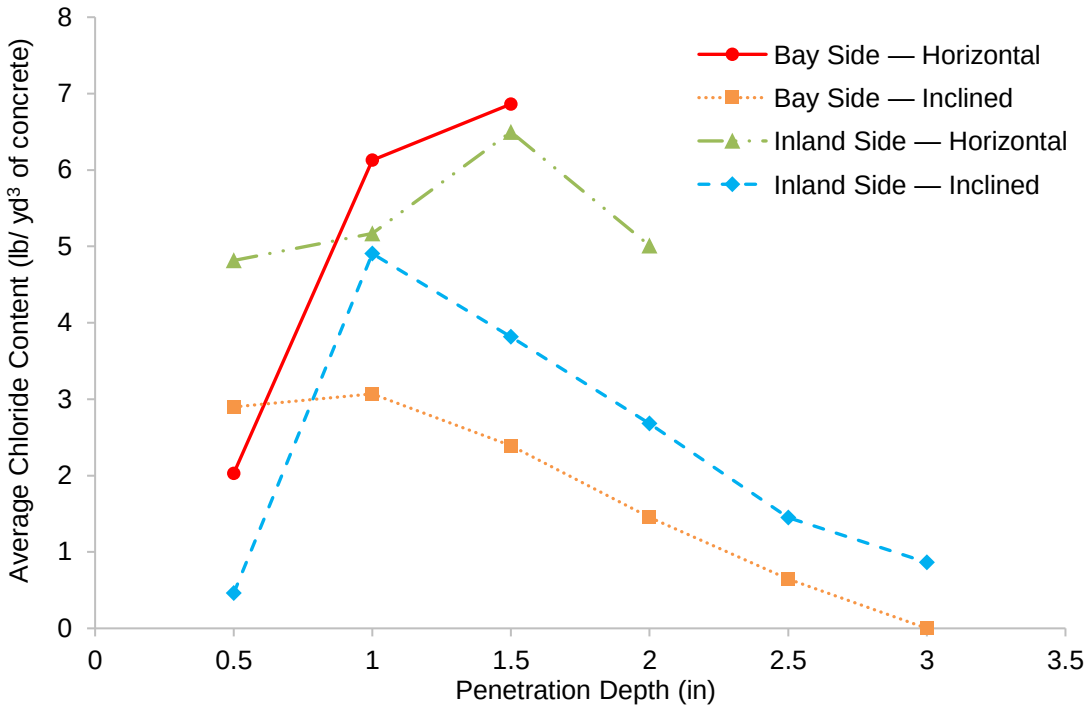

Figure 77. Results of Chloride Testing for I-Beam 6

I-Beam 3 – Bad Condition

The results of chloride content testing for I-Beam 3 are shown and Figure 78. Figure 13 shows the locations of the extracted samples on I-Beam 3. As a general trend, the chloride content in both the inclined and horizontal samples were the highest near the concrete surface and decreased gradually with deeper samples. However, for the inland side inclined and bay sides, the penetration depth of 1 in had a higher chloride content than the starting depth 0.5 in. This can be explained by the fact that water or rain could probably wash off chloride content at the concrete surface which resulted in a low reading. The highest chloride content was found in the bay side with (5.6 lb/yd^3) which is considered in a high risk of corrosion category.

Box Beam 1 – Good Condition

The results of chloride content testing for Box-Beam 1 are shown in Figure 79. Figure 14 shows the locations of the extracted samples on Box Beam 1. As can be seen from the graph, the chloride content of the top portion of the box beam had the lowest chloride content compared to the east side and the west side. This result can be explained by the fact that the top of the box beam was covered with an asphalt overlay that was a first line of defense against chloride penetration. Additionally, cracks are known to form in the top surface and along the longitudinal

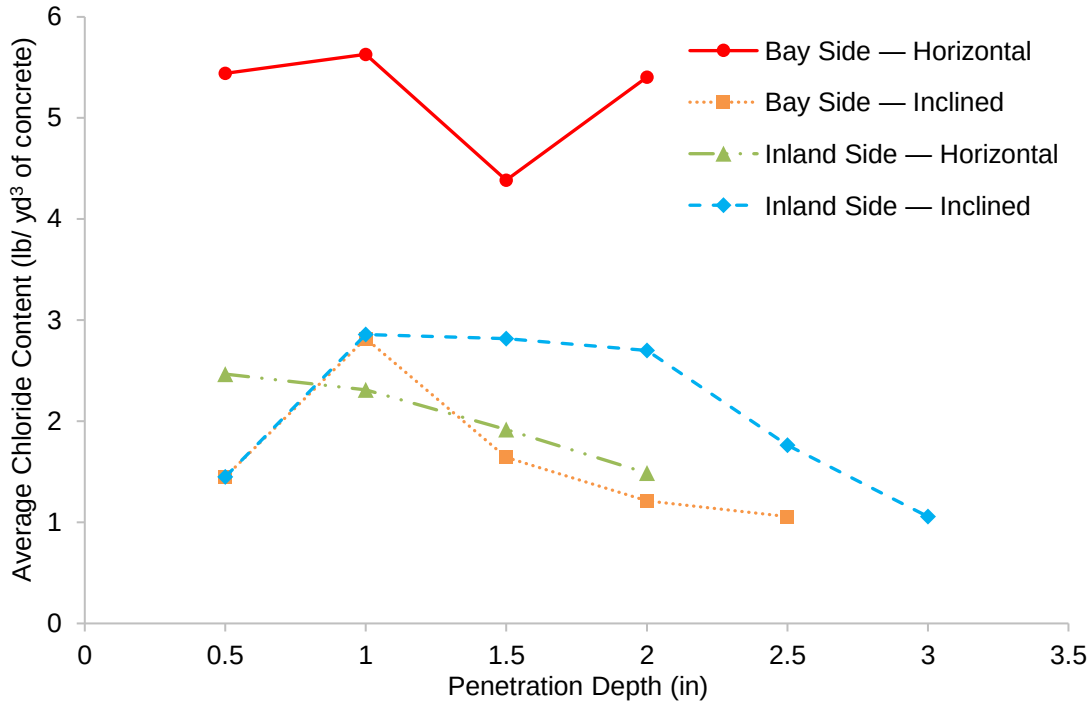

Figure 78. Results of Chloride Testing for I-Beam 3

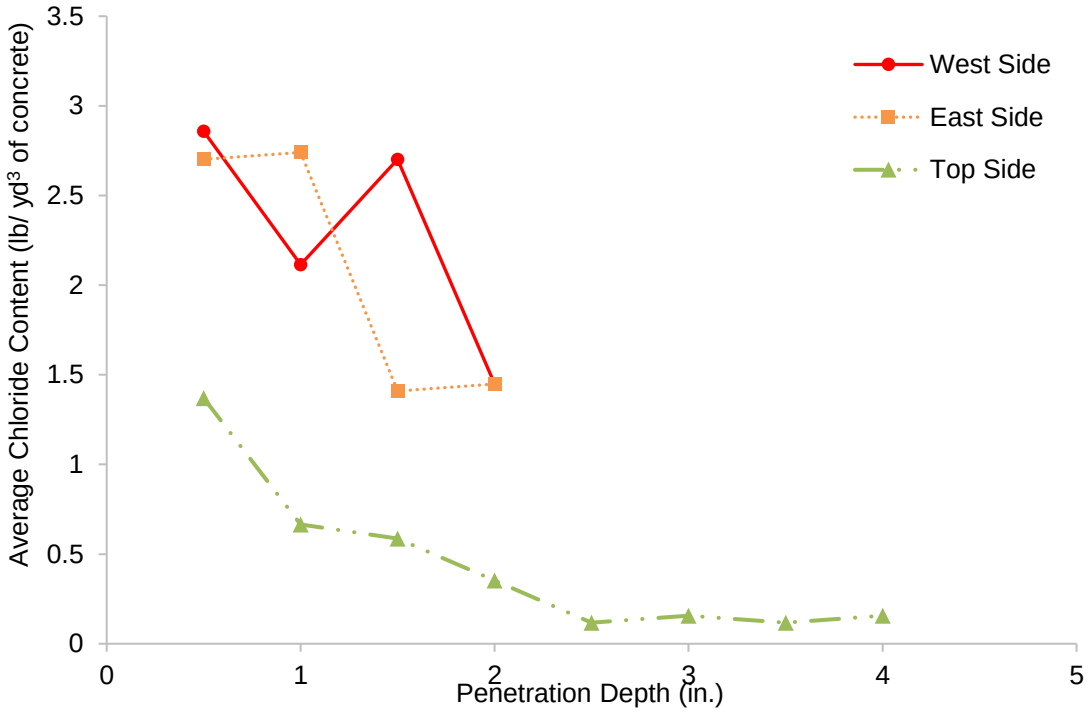

Figure 79. Results of Chloride Testing for Box Beam 1

joints between adjacent precast box beams. These longitudinal cracks provide a direct path for chloride-laden water to reach the side and bottom of the beams. Similar to all other beams, the chloride contents gradually decreased as the depth of the sample increased. For the west side, the highest chloride content was at a depth of 0.5 in and lowest at a depth of 2.0 in. While for the east side, the highest and lowest chloride content was at 1.0 in and 1.5 in, respectively.

Box Beam 4 – Medium Condition

The results of chloride content testing for Box Beam 4 are shown in Figure 80. Figure 15 shows the locations of the extracted samples on Box Beam 4. The west side had the highest chloride content at 1.0 in depth, and the chloride content fluctuates as the depth increase. There was no detected chloride content for the east side. For the top side, the chloride content was very low with 0.313 lb/yd^3 at 2.5 in and 0.235 lb/yd^3 at 3.5 in. One possible explanation is that these box beams had been stored outside for more than five years, allowing rain water to wash off much of the chlorides at the shallow depths.

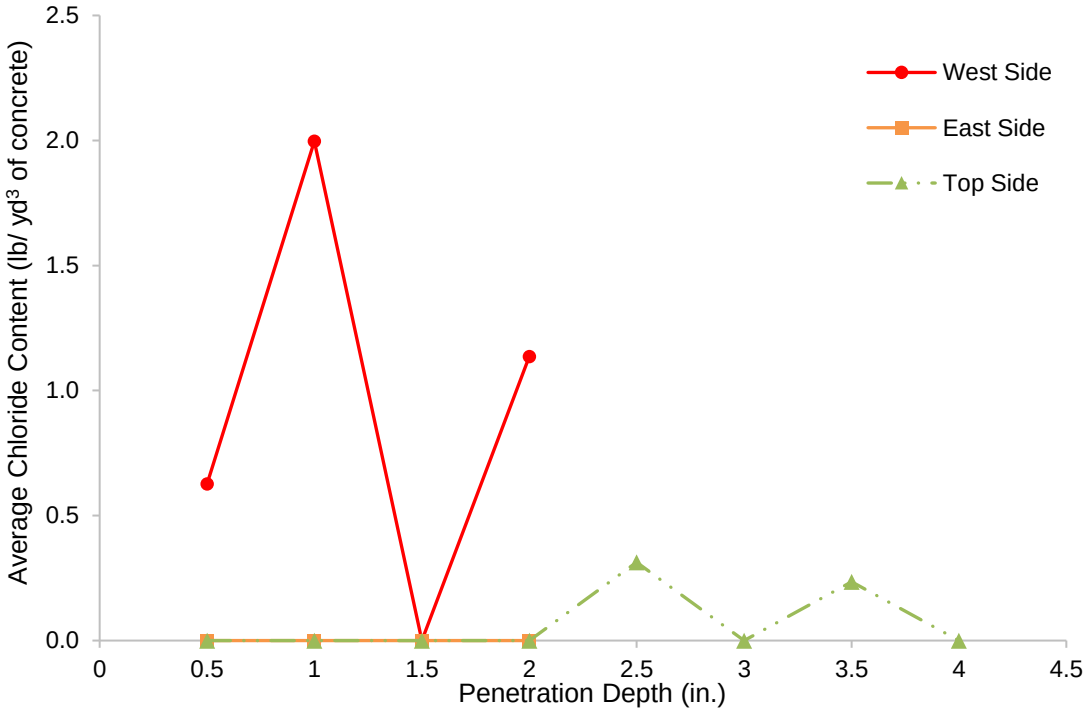

Figure 80. Results of Chloride Testing for Box Beam 4

Box Beam 2 – Bad Condition

The results of chloride content testing for Box Beam 2 are shown in Figure 81. Figure 16 shows the locations of the extracted samples on Box Beam 2. As can be seen in the graph, overall, the west side had the highest chloride content at 1.0 in depth. The second highest chloride content was the east side at 0.5 in and 1.0 in. For the top section, the chloride content was the lowest compared to the other parts of the concrete. For all of the sections, as a general trend, the chloride content decreased gradually with depth of the sample.

Comparison of Chloride Contents at the Level of the Strands

For each beam, the worst case chloride concentration was compared to the risk of corrosion as presented in Table 7 and the assessed condition of the beams based on visual inspections. The comparison is presented in Table 8.

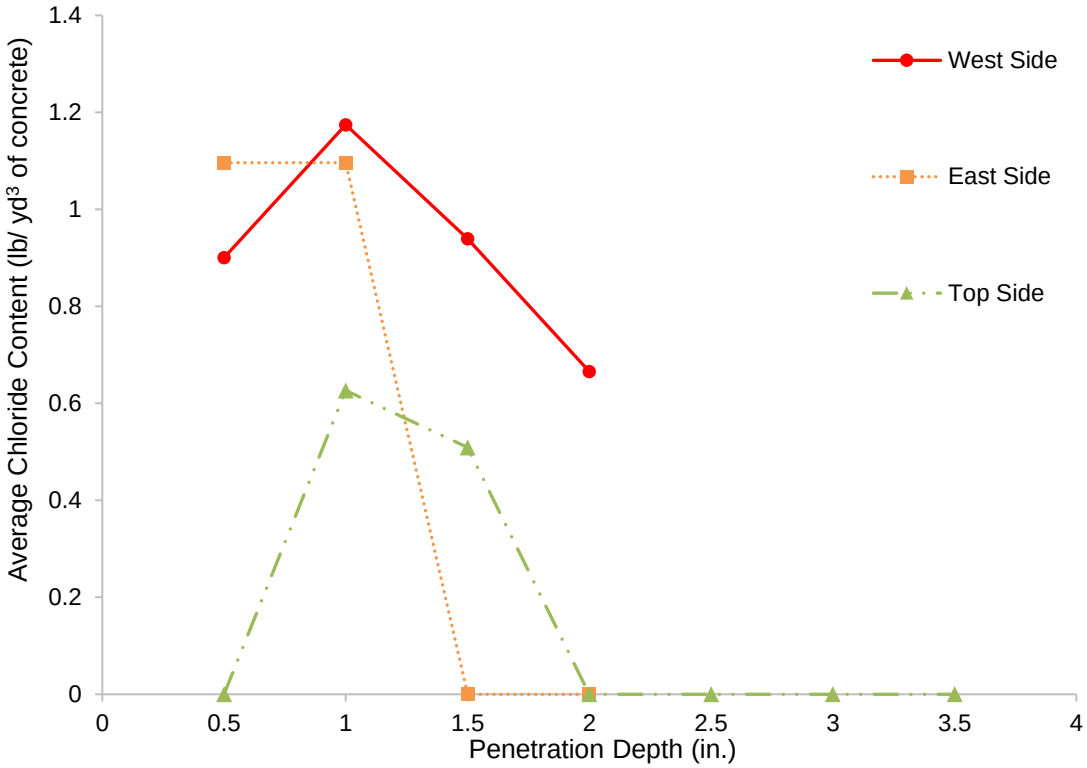

Figure 81. Results of Chloride Testing for Box Beam 2

Table 8. Comparison of Chloride Tests and Visual Inspection Evaluations

Beam Designation	Assessed Condition from Visual Inspection	Chloride Concentration at Strand Level, lb/yd^3	Risk of Corrosion
I-Beam 7	Good	4.39	Medium
I-Beam 6	Medium	5.01	Medium
I-Beam 3	Bad	5.40	Medium
Box Beam 1	Good	1.45	Low
Box Beam 4	Medium	1.14	Negligible
Box Beam 2	Bad	0.67	Negligible

The chloride concentrations from all of the I-Beams indicate a medium risk of corrosion, and yet they had very different levels of corrosion damage to their strands. I-Beam 7, which had the lowest concentration, had almost no evidence of corrosion of the strands. I-Beams 6 and 3, had higher chloride concentrations, and more evidence of corrosion damage. The Box Beams also gave odd results. The chloride concentrations indicated a low to negligible risk of corrosion, and yet all three beams showed evidence of significant corrosion of the strands.

Compressive Strength Testing

The compressive strength was measured for each concrete core sample. The results are presented in Table 9. The design concrete strengths for the slab and I-beam were 3.5 ksi and 4 ksi, respectively. However, the average concrete strength of the deck after nearly 50 years of

service was slightly lower than that specified in the plans, with the exception of I-beam 7, which was relatively high at 7.2 ksi. All of the cores indicated that the original deck included river gravel, and a later overlay was made from latex modified concrete. It is unknown why the core from the deck of I-beam 7 was so much stronger than the others. Regarding the I-beams, the concrete strength was higher than the original plan strength by 45%. Similarly, the 33-year old box beams had a compressive strength that was 40% higher than the 5-ksi design strength.

Table 9. Compressive Strength for Concrete Cores

Beam/Sample	Length (in)	Dia-meter (in)	H/D	Load (lb)	Area (in^2)	Compressive strength (psi)	Factored Compressive Strength (psi)	Average Factored Compressive Strength (psi)
I-Beam 6 Flange Sample 1	6.50	3.25	2.00	22500	8.29	2712	2712	2860
I-Beam 6 Flange Sample 2	6.50	3.25	2.00	25000	8.29	3014	3014	
I-Beam 6 Web Sample 1	5.25	2.75	1.90	32500	5.93	5472	5472	6100
I-Beam 6 Web Sample 2	5.20	2.75	1.89	40000	5.93	6734	6734	
I-Beam 3 Flange Sample 1	6.30	3.25	1.93	28000	8.29	3375	3375	3500
I-Beam 3 Flange Sample 2	6.30	3.25	1.93	30000	8.29	3616	3616	
I-Beam 3 Web Sample 1	5.80	2.75	2.10	32500	5.93	5472	5472	5600
I-Beam 3 Web Sample 2	5.80	2.75	2.10	34000	5.93	5724	5724	
I-Beam 7 Flange Sample 1	7.00	4.00	1.75	87500	12.50	6963	6824	7230
I-Beam 7 Flange Sample 2	6.00	4.00	1.50	100000	12.50	7958	7639	
I-Beam 7 Web Sample 1	3.60	2.75	1.30	35000	5.93	5893	5516	5870
I-Beam 7 Web Sample 2	5.00	2.75	1.81	37000	5.93	6229	6229	
Box-Beam 1 Sample 1	4.25	2.75	1.54	43000	5.93	7240	6972	7300
Box-Beam 1 Sample 2	4.00	2.75	1.45	47500	5.93	7997	7629	
Box-Beam 2 Sample 1	5.00	2.75	1.81	45000	5.93	7576	7576	7200
Box-Beam 2 Sample 2	3.85	2.75	1.40	43000	5.93	7240	6863	
Box-Beam 4 Sample 1	4.20	2.75	1.52	45000	5.93	7576	7281	6630
Box-Beam 4 Sample 2	3.80	2.75	1.38	39000	5.93	6566	6205	
Box-Beam 4 Sample 3	4.90	2.75	1.78	38000	5.93	6398	6398	

Tension Testing

Table 10 shows the yield and ultimate tensile strengths of the prestressing strands that were extracted from the end of each beam. As specified in the plans, 7/16-in, stress-relieved grade 270 strands were used in all of the beams. Figures 82 through 93 show the stress-strain relationships and photographs of the prestressing strands. In the plots of stress-strain behavior, the tensile tests results are compared to the stress-strain model which was used in the calculation of the capacity of the beams. The condition of the strands varied from beam to beam. Some of them were heavily damaged, such as the strand from I-beam 6 and all box beams, while strands from I-beam 3 were in a good condition. I-Beam 7 strand had light damage.

Table 10. Tensile Test Results

Strand No.	Girder Designation	Elastic Modulus, ksi	Yield Strength, ksi	Ultimate Strength, ksi
1	I-Beam 7	31,000	243.5	261.5
2	I-Beam 6	27,500	N.A	188.5
3	I-Beam 3	34,000	252	272
4	Box Beam 1	33,000	257	269
5	Box Beam 2	30,000	N.A	224
6	Box Beam 4	N.A	90	191

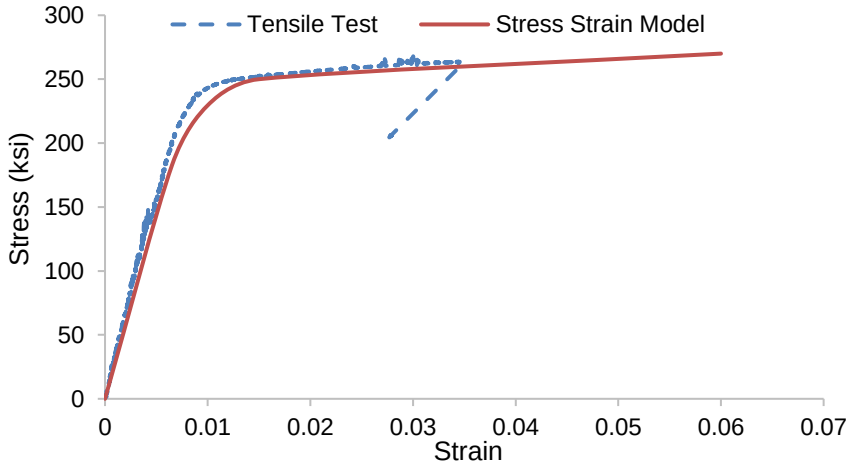

Figure 82. Stress-Strain Behavior of Strand Taken from I-Beam 7

Figure 83. Strand Taken from I-Beam 7 after Testing

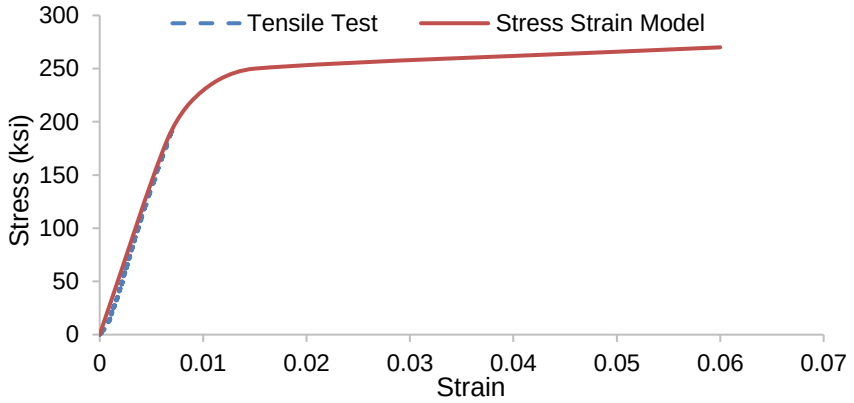

Figure 84. Stress-Strain Behavior of Strand Taken from I-Beam 6

Figure 85. Strand Taken from I-Beam 6 after Testing

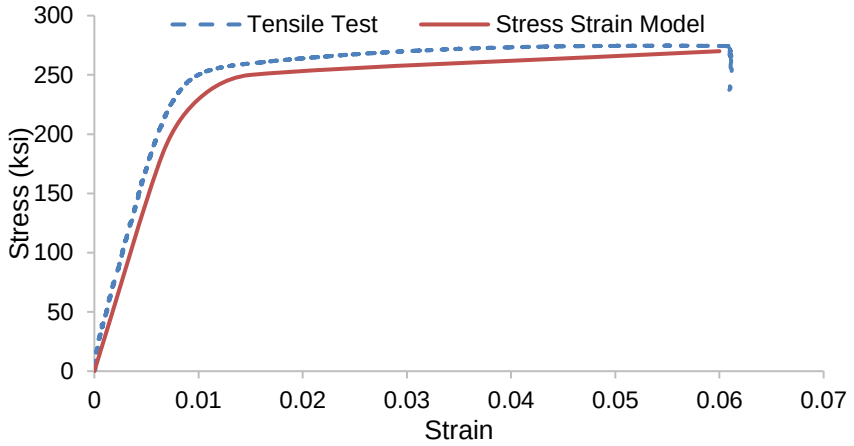

Figure 86. Stress-Strain Behavior of Strand Taken from I-Beam 3

Figure 87. Strand Taken from I-Beam 3 after Testing

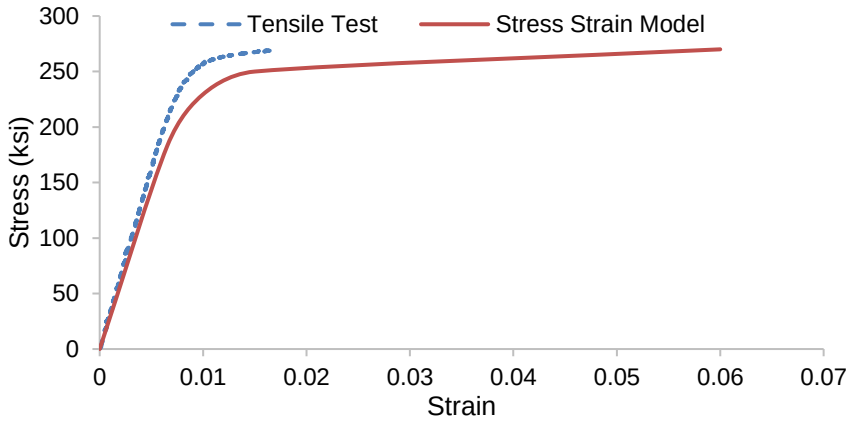

Figure 88. Stress-Strain Behavior of Strand Taken from Box Beam 1

Figure 89. Strand Taken from Box Beam 1 after Testing

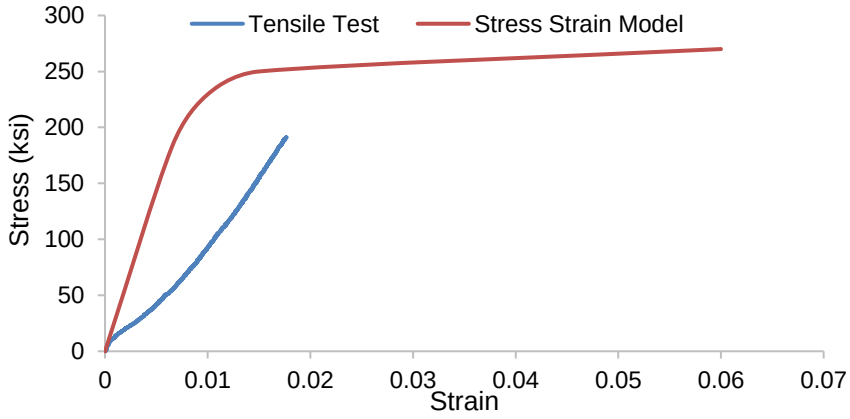

Figure 90. Stress-Strain Behavior of Strand Taken from Box Beam 4

Figure 91. Strand Taken from Box Beam 4 after Testing

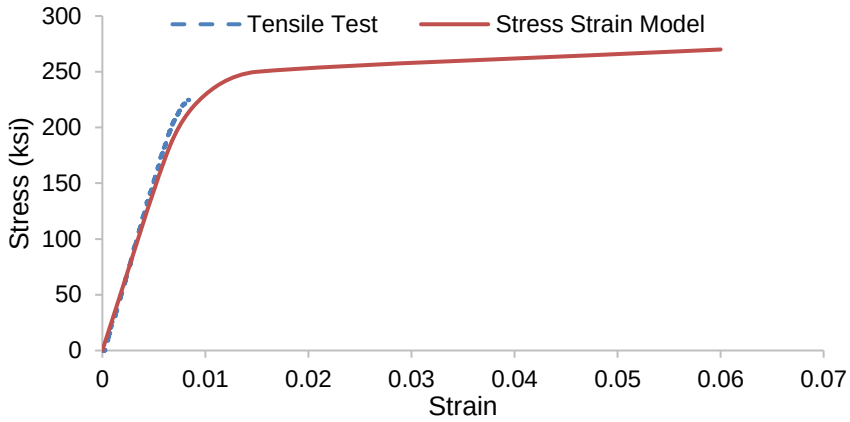

Figure 92. Stress-Strain Behavior of Strand Taken from Box Beam 2

Figure 93. Strand Taken from Box Beam 2 after Testing

All the tensile tests were very similar to the stress strain model, prior to yield, except for the strand from Box Beam 4. The strands extracted from I-beam 6 and all three box beams failed to reach a strain of 0.02, because of their heavy corrosion. The stress-strain behavior of the strand from I-beam 3 was identical to the stress strain model, because it did not show any signs of damage. The strand from I-beam 7 did not achieve the expected ultimate strain, but also had light corrosion on its surface.

Analysis of Data and Development of Method for Residual Strength Calculation

This section presents the results of the calculations performed to predict the flexural strength of each beam using four approaches for each beam. Two methods were used to determine a reduced area of prestressing strand to use in the calculations to reflect the corrosion damage. The two methods were the recommendations of Naito et al. (2010), and a modified method described below. With each reduced prestressing area, strength was calculated once using a strain compatibility approach, and again using the simplified method from the AASHTO LRFD Bridge Design Specifications (2017).

Modified Method for Estimating Strength of Corrosion Damaged I-Beams

The modified method developed in this study and used to calculate the strength of each beam is presented in this section. Types of damage to be considered in this method included longitudinal cracking, delamination, patching, exposed strands and spalled sections. This method was developed by relating the visually inspected I-beams to the flexural tests results from this

study. The following guidelines were used to determine the residual capacity for prestressed I-beams.

All types of damage that are within a distance of a strand's development length away from the section being evaluated should be considered for load rating purposes. The AASHTO development length equation should be used as a reference. All of the following guidelines were used to estimate the strength reduction due to corrosion:

- *For Regions of Beams With Longitudinal Cracking:* A given strand's original cross-sectional area should be reduced as follows:
  1. By 40%, for strands directly in line of the crack (Figure 94).
  2. By 20%, for strands within concrete cover distance to the exterior surface adjacent to the longitudinal crack (Figure 94).

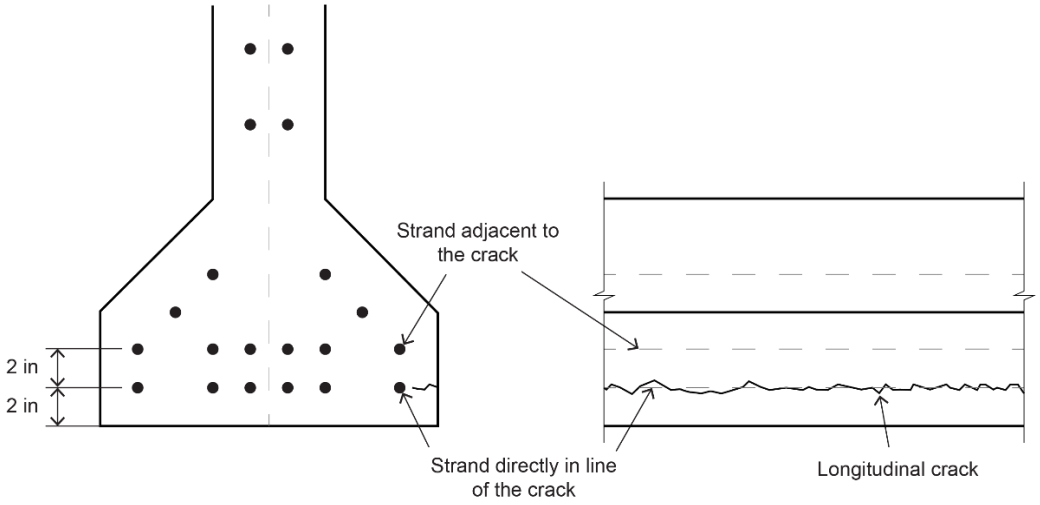

Figure 94. Cross-section and elevation view for I-Beam

- *For Regions of Beams With Delaminations:* All strands in the delaminated area should be reduced to 80% of the original cross-sectional area for capacity calculation. Since most delaminations originate at the layer of strands closest to the surface, it can be assumed that only this layer of strands is within the delaminated area.

- *For Regions of Beams With Spalled Area:* If the spalled section does not include exposed strands, no reduction should be used. If it contains exposed strands, the following should be used:
  1. If the condition of the exposed strands is heavily corroded or cut, disregard the full strength of the exposed strand.
  2. If the condition of the exposed strands is moderate, a reduction of 80% of the original cross-sectional area of the exposed strand shall be considered in the capacity calculation.

- *For Regions of Beams With Patched Area:* A reduction to 10% of the original cross-sectional area is recommended for all the strands in the patched area.

This modified method was used for the strength calculation of all I-beams. For the box beams, however, the result using the modified method closely resembled the results using the recommendations of Naito et al. (2010), but they did not match the test results as well. Therefore, only the Naito et al. (2010) recommendations were used for analyzing the box beams.

Comparison of Calculation Methods to Test Results

I-Beam 7 – Good Condition

Based on all observations and non-destructive tests, this beam appeared to be in very good condition, with no visible corrosion damage to any strands. Therefore, the strength was calculated using the cross-section shown in Figure 95. More detail on the reinforcement in the deck and other dimensions can be found in Figure 23. The haunch at mid-span was 1.5 in. The slab concrete strength was 7200 psi, and the beam concrete strength was 5800 psi. The results of the strength calculations using strain compatibility and the AASHTO method are shown in Table 11.

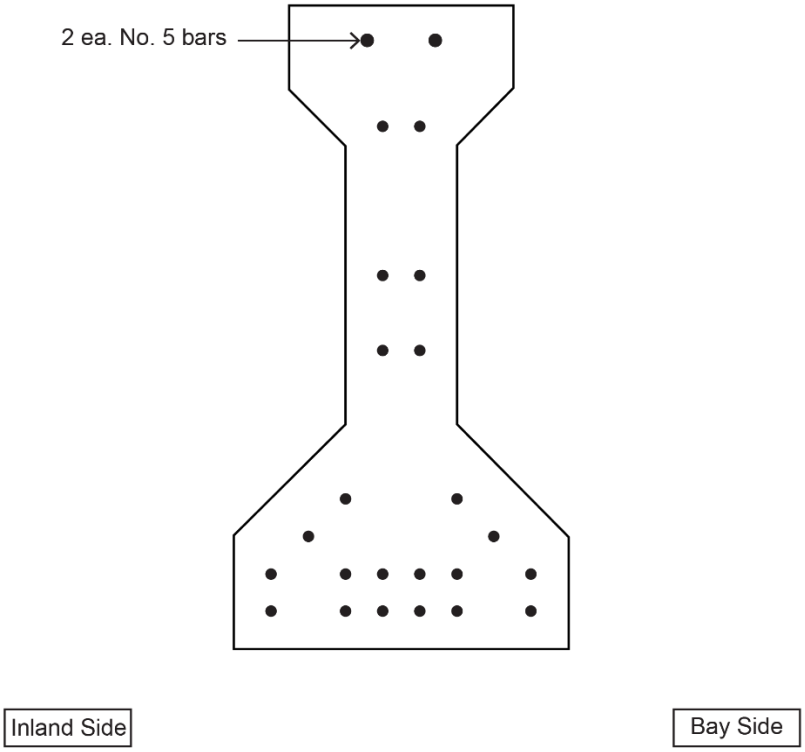

Figure 95. Cross-section for I-Beam7

Table 11. Estimates of Strength Assuming No Damage of I-Beam 7

Damage Estimate Method	Strength Calculation Method	Flexural Strength k-ft
As-Tested	Test Data	2038
Assumed No Damage	AASHTO	2017
	Strain Compatibility	2034

The failure load for this beam was 182 kips. Based on the 48-ft span length and the 8-ft spreader beam, the applied moment at mid-span was 1820 k-ft. In addition, the beam was carrying its own self weight and deck weight, which caused a mid-span moment of 218 k-ft. Thus, the total mid-span moment at ultimate capacity was 2038 k-ft, which is only slightly higher than the calculated strength from either the strain compatibility method or the AASHTO method. Thus, the analysis validated the methods and material properties used for the calculation of strength and confirmed that this beam did not have any strength degradation due to corrosion damage. See Table 11 for a comparison of the results for this beam.

I-Beam 6 – Medium Condition

The strength for this beam was calculated using two methods to account for the damage: the recommendations of Naito et al. (2010), and the modified method. The damage inferred from the pre-test visual inspection is presented in Figure 96. The calculations were performed with the tested deck concrete strength of 2900 psi and the beam concrete strength of 6100 psi. The haunch at mid-span was 1.5 in. The tested strength of this beam was 1393 k-ft. The calculations using strain compatibility and the AASHTO method are presented in Table 12. Based on the damage maps, two out of six strands in the first lower level were in a patched area, and the other two had longitudinal cracks. Additionally, one strand out of six in the second lower level was in the patched area.

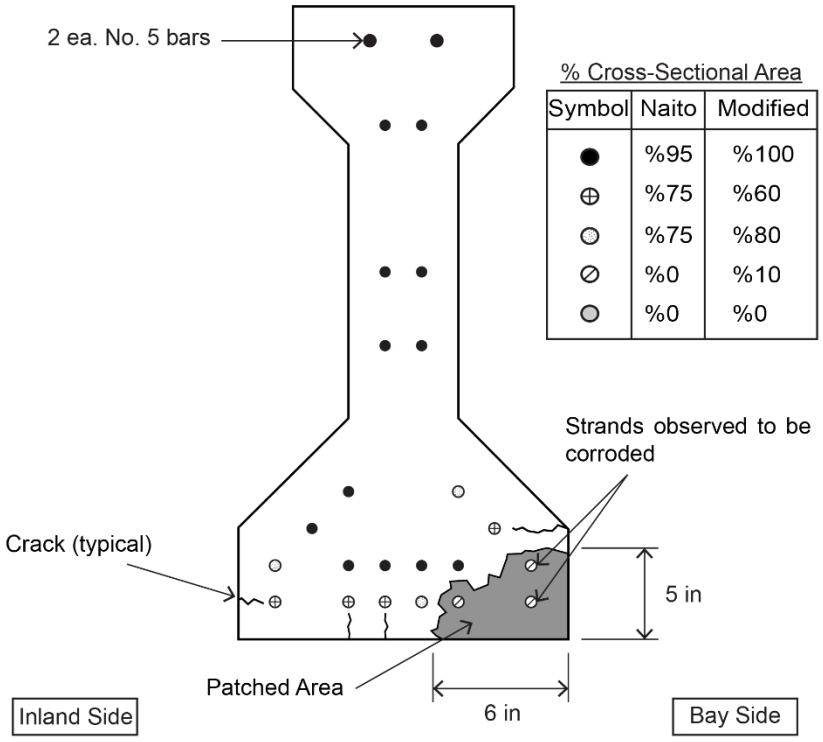

Figure 96. Damage Estimated from Visual Inspection for I-Beam 6

In order to calculate the flexural strength for both damage estimate methods, the effective prestress was calculated by assuming prestress losses as prescribed by AASHTO. As an aside, this AASHTO-calculated value of 151.4 ksi was compared to the effective prestress calculated

Table 12. Estimates of Strength Considering Damage of I-Beam 6

Method to Estimate Damage	Method to Calculate Strength	Flexural Strength, k-ft
Experimental Test		1393
Naito et al. (2010)	AASHTO	1377
	Strain Compatibility	1402
Modified Method	AASHTO	1401
	Strain Compatibility	1428

for both damage estimation methods using the experimental cracking load of 70 kips. The effective prestress values were 177.5 ksi, and 141 ksi, for the Naito et al. and modified methods, respectively.

As can be seen in Table 12, the Naito et al. method and modified method provided slightly unconservative estimates of residual strength using the strain compatibility method. They overestimated the strength by 0.6 and 2.5% respectively. Using the AASHTO method, the Naito et al. method provided a conservative estimate of residual strength, underestimating the strength by 1.1%, while modified method overestimated by 0.6%.

I-Beam 3 – Bad Condition

Naito et al. (2010) and the modified method were used to account for the damage in I-Beam 3 (see Figure 98). Prior to testing, there was one exposed strand in the first lower level. The deck concrete strength was 3500 psi and the beam concrete strength was 5600 psi. The haunch at mid-span was 1.5 in. The tested strength of this beam was 1873 k-ft. The effective

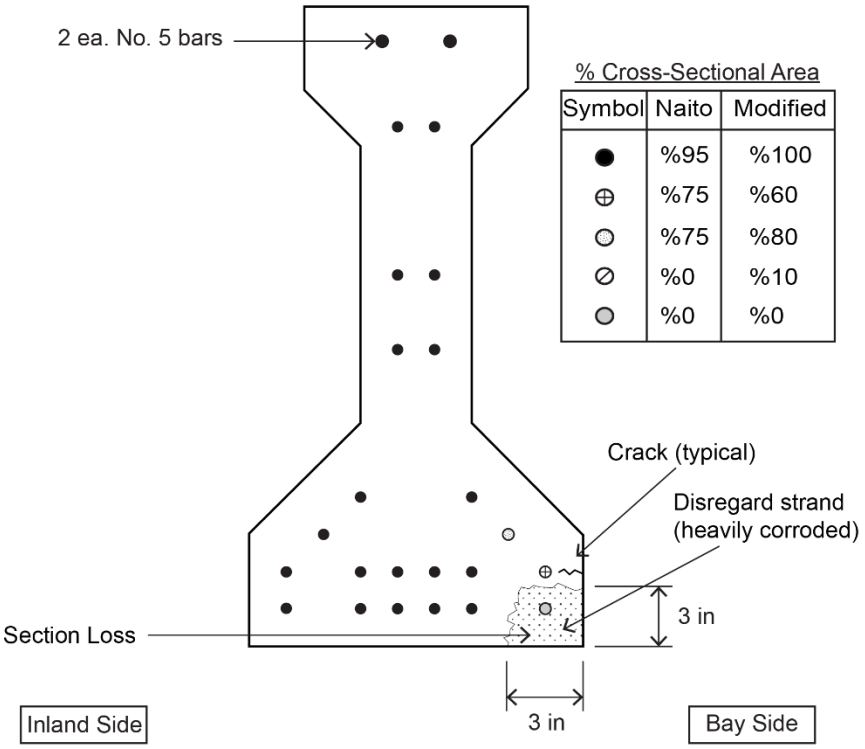

Figure 98. Damage Estimated from Visual Inspection for I-Beam 3

prestress calculated using the AASHTO method of prestress losses was 150 ksi; this value was used in the strain compatibility method for calculating the flexural strengths for each damage estimation method. See Table 13 for the results. The effective prestress calculated from the observed actual cracking load (50 kips) was 142 ksi using the modified calculations and 152 ksi using the Naito et al. (2010) damage estimate.

Table 13. Estimates of Strength Considering Damage of I-Beam 3

Method to Estimate Damage	Method to Calculate Strength	Flexural Strength, k-ft
Test		1873
Naito et al. (2010)	AASHTO	1675
	Strain Compatibility	1699
Modified Method	AASHTO	1735
	Strain Compatibility	1762

Box Beam 1 – Good Condition

The cross-sectional area of the strands in Box Beam 1 to be used for calculations were assumed using the recommendations of Naito et al. (2010). Based on visual inspection, three exposed strands in the first lower level were heavily corroded (see Figure 99). Those assumptions, along with the tested concrete strength of 7250 psi, resulted in estimated flexural strengths that were within about 1% the actual strength determined from load testing. The total moment on the beam during testing, including self-weight, was 1269 k-ft. Using strain compatibility, the calculated flexural strength was 1253 k-ft, while the capacity at ultimate using the AASHTO method was slightly lower at 1251 k-ft. Note that the effective prestress calculated from the AASHTO method was 156 ksi. On the other hand, the effective prestress calculated from the observed 50-kip cracking load and the Naito et al. (2010) recommendations was 128 ksi, which was about 18% below the AASHTO-based effective prestress.

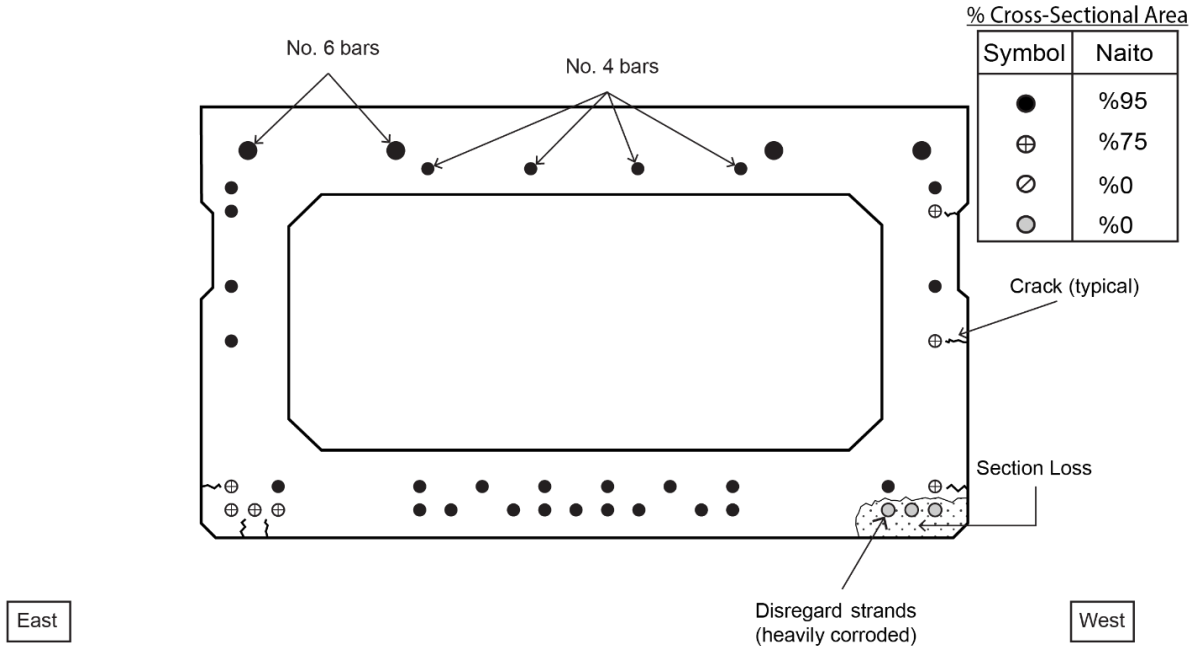

Figure 99. Damage Estimated from Visual Inspection for Box Beam 1

Box Beam 4 – Medium Condition

Box Beam 4 had different conditions than the other two box beams, with water trapped in the beam leading to a lower strength. The recommendations of Naito et al. (2010) were used with a small modification to account for the trapped water, where a 15% reduction was applied on top of the Naito reductions to the two lower strands levels (see Figure 100). This percentage reduction gave reasonable calculated results. Based on the compressive test, the concrete strength was 6250 psi. The tested strength of this beam was 1196 k-ft. The calculations using strain compatibility and the AASHTO method are presented in Table 14. Note that the actual cracking load of 50 kips resulted in an effective prestress equal 167 ksi. On the other hand, the effective prestress calculated from the AASHTO method was 156 ksi. This latter value for effective prestress was used in the strain compatibility calculation method for flexural strength.

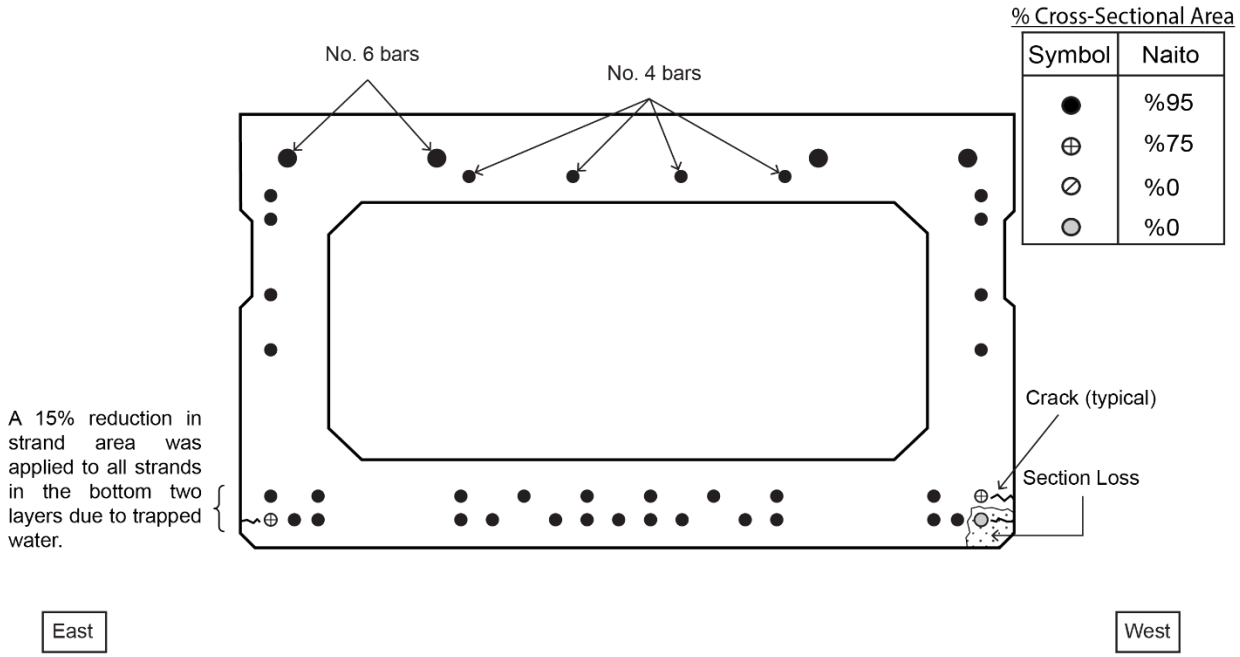

Figure 100. Damage Estimated from Visual Inspection for Box Beam 4

Table 14. Estimates of Strength Considering Damage of Box Beam 4

Method to Estimate Damage	Method to Calculate Strength	Flexural Strength, k-ft
Test		1196
Naito et al. (2010)	AASHTO	1342
	Strain Compatibility	1367
Naito et al. (2010) (trapped water reduction is included)	AASHTO	1181
	Strain Compatibility	1185

Box Beam 2 – Bad Condition

The residual capacity for Box Beam 2 was calculated using the recommendations of Naito et al. (2010) to estimate the remaining cross-sectional area of the strands. Three exposed strands were disregarded in the calculation of the flexural strength (see Figure 101). The concrete

strength used in the calculation was 7100 psi which was obtained from compression tests of extracted cores. The tested strength of this beam was 1284k-ft. Following the strain compatibility method, the flexural strength was calculated to be 1292 k-ft. Using the AASHTO method resulted in a moment equal to 1289 k-ft. Based on the actual cracking load (49 kips), the effective prestress calculated was 146 ksi. On the other hand, the effective prestress calculated from the AASHTO method was 156 ksi.

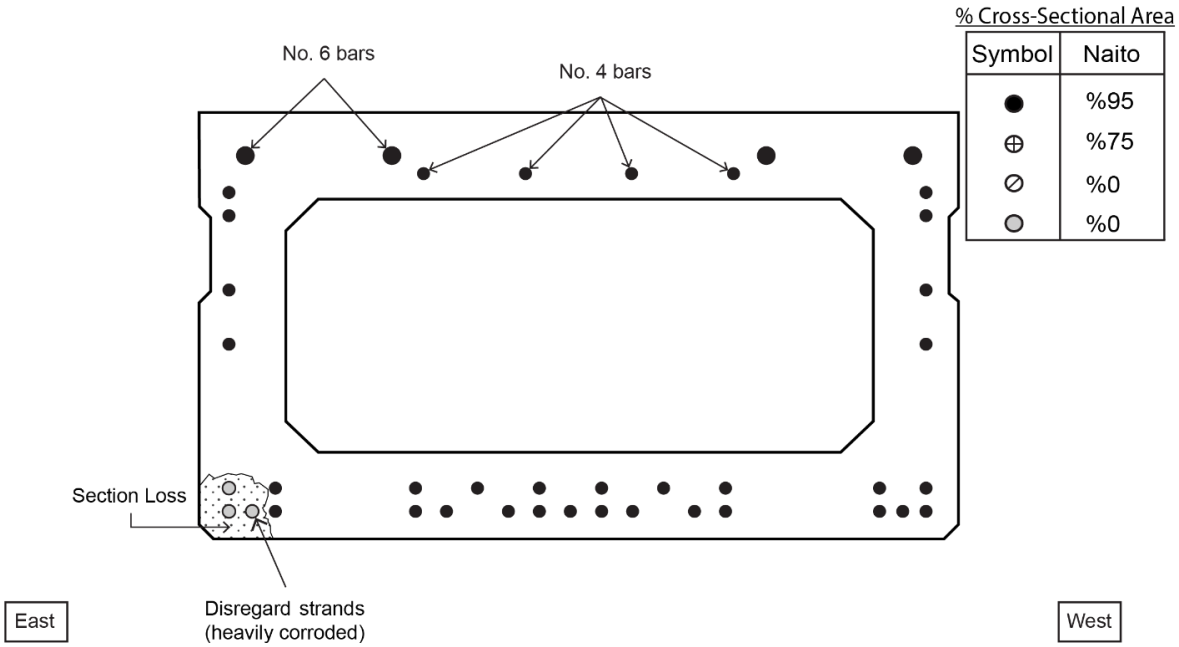

Figure 101. Damage Estimated from Visual Inspection for Box Beam 2

Summary of Performance of Damage Assessments

For all of the beams in this study, Table 15 compares the results of assuming reduced cross-sectional areas of prestressing steel, as dictated by the Naito et al. and the modified method, when calculating the flexural strength using the strain compatibility method. Note that for box beams, only the Naito et al. method was used. Table 16 makes the same comparisons, except using the AASHTO method for the calculation of the stress in the strands at ultimate. From the tables, all methods provided reasonable estimates of residual flexural strength, with the Naito et al. method being more conservative for the I-beams as compared to the modified method. The Naito et al. method provided very accurate estimates of residual strength for Box Beam 2 and Box Beam 1, but was unconservative for Box Beam 4. As discussed previously, the water trapped inside of Box Beam 4 contributed to additional unseen corrosion damage and associated loss of strength.

DISCUSSION

The primary input required to calculate a reasonable estimate of residual strength of corrosion-damaged prestressed bridge beams is a good map of the damage observed during a detailed safety inspection. Previous patching, longitudinal cracking along the strands,

Table 15. Comparison of Methods to Tests Using Strain Compatibility

Beam	Tested Strength k-ft	Naito et al. (2010)		Modified Method	
		Estimated Strength, k-ft	M_{test} / $M_{estimated}$	Estimated Strength, k-ft	M_{test} / $M_{estimated}$
I-Beam 7 - Good	2038	2034	1.00	2034	1.00
I-Beam 6 - Medium	1393	1402	0.99	1428	0.97
I-Beam 3 - Bad	1873	1699	1.10	1762	1.06
Box Beam 1 - Good	1269	1253	1.01	N/A	N/A
Box Beam 4 - Medium	1196	1367	0.87	N/A	N/A
Box Beam 2 - Bad	1284	1292	0.99	N/A	N/A

Table 16. Comparison of Methods to Tests Using AASHTO Strength Calculations

Beam	Tested Strength k-ft	Naito et al. (2010)		Modified Method	
		Estimated Strength, k-ft	M_{test} / $M_{estimated}$	Estimated Strength, k-ft	M_{test} / $M_{estimated}$
I-Beam 7 - Good	2038	2017	1.01	2017	1.01
I-Beam 6 - Medium	1393	1377	1.01	1401	0.99
I-Beam 3 - Bad	1873	1675	1.12	1735	1.08
Box Beam1 - Good	1269	1251	1.01	N/A	N/A
Box Beam 4 - Medium	1196	1342	0.89	N/A	N/A
Box Beam 2 - Bad	1284	1289	0.99	N/A	N/A

delamination, and concrete spalls are all excellent evidence that strand corrosion has progressed to a point where the strand in the deteriorated region cannot be completely counted on to contribute to flexural strength. The half-cell potential measurements, did not provide any additional information to inform the calculation of strength. This is in agreement with the findings of Naito et al. (2010), which found that there was some correlation between half-cell results and corrosion of strands, but the coefficient of variation of tests was very high.

The post-test destructive evaluations were valuable to determine concrete strength and strand stress-strain properties. However, the chloride concentration results were mixed. As shown in Table 8, the results showed only negligible to low probability of corrosion in the box beams, while in reality they all had at least a few exposed and broken strands. Chloride concentrations also indicated that all of the I-beams had a medium probability of corrosion, but I-beam 7 showed almost no evidence of active corrosion. So, this type of tests is not valuable for evaluating damage for a strength estimation.

To provide the engineer the required information for an accurate estimate of residual strength, bridge inspectors need to develop detailed damage maps, such as those shown in Figures 25 through 30. The locations of the various types of damage need to be carefully documented so the load rater can employ the damage estimation recommendations in their strength calculations. Many inspectors already provide these types of detailed maps.

CONCLUSIONS

- *For prestressed I-beams, either the AASHTO simplified method or strain compatibility approach can be used with the Naito et al. (2010) method of damage estimation to calculate*

conservative estimates of flexural strength. The modified method for damage estimation, as presented in this report, provides slightly more accurate, but sometimes slightly unconservative, estimates of residual strength compared to the Naito et al. (2010) method.

- *The Naito et al. (2010) recommendations to estimate the residual cross-sectional area of prestressed strands in adjacent box beams result in reasonably accurate estimates of strength.*

- *Poor drainage of water from the inside of box beams can lead to hidden damage, resulting in overly optimistic predicted flexural strength.*

- *Data collected from visual inspections are the best inputs and are sufficient for estimating the remaining cross-sectional area of strands in prestressed concrete flexural members.* For unknown reasons, half-cell potentials, resistivity measurements and chloride concentration testing did not provide consistent results in this study.

RECOMMENDATIONS

1. *VDOT's Structure and Bridge Division should follow the Naito et al. (2010) method of damage estimation with either the AASHTO simplified method or strain compatibility approach, as presented in this report, to estimate damage and perform load ratings of corrosion damaged I-beams.*

2. *VDOT's Structure and Bridge Division should follow the Naito et al. (2010) recommendations to estimate damage and then perform load ratings of corrosion-damaged adjacent box beams using either the AASHTO simplified method or strain compatibility approach.*

3. *When performing routine bridge safety inspections, VDOT's Structure and Bridge Division should have their bridge inspectors create detailed maps of corrosion-damaged beams, including size and location of all cracks, spalls, delaminations and patches.*

4. *VDOT's Structure and Bridge Division should have their bridge inspectors confirm the presence of weep holes in box beam bridges during routine inspections and make sure that they are clear and allowing proper drainage of water. If large quantities of water drain from any location in the bridge, this should be clearly noted in the inspection report.*

IMPLEMENTATION AND BENEFITS

Implementation

With regards to recommendations 1 and 2, VDOT's Structure and Bridge Division has requested detailed examples for estimating the remaining cross-sectional area of corrosion-damaged prestressing strands, as well as example computations for the flexural capacity of prestressed concrete bridge girders based on those cross-sectional estimates. Upon receipt of the

calculations, the Structure and Bridge Division will implement these two recommendations, with the objective implementation date being March 2027.

With regards to recommendation 3, VDOT inspectors already create detailed maps of damage as a part of standard practice, per the National Bridge Inspection Standards. Thus, this recommendation does not need any further implementation.

With regards to recommendation 4, VDOT's Structure and Bridge Division has already incorporated guidance for the maintenance of weep holes in prestressed concrete box beams in Part 2: Design Aids and Typical Details, Chapter 32: Preservation, Maintenance, Repair, Widening and Rehabilitation, of the *VDOT Manual of the Structure and Bridge Division*. Furthermore, the recommended inspection procedure and documentation of the weep hole condition can be handled by the inspection processes that are already in place.

Benefits

If *recommendations 1* and *2* were to be implemented for estimating the reduced cross-sectional areas for strands that are not yet visible, the results may yield lower strength estimations compared to those calculated with existing methods, depending on what percent of strength is currently being used for these strands. If those recommendations result in lower strength estimates, additional costs may be incurred from maintenance, repair or bridge postings. However, the benefit is in knowing that the strength estimates are conservative and the safety of the motoring public is more secure.

There should be no added costs associated with *recommendation 3* and developing detailed damage mapping, provided that this type of reporting is already being performed by bridge inspectors.

Likewise, there will be no costs in implementing *recommendation 4* given that such activity is already taking place during routine preventative maintenance on the structure. On the other hand, the benefit to clearing weep holes for drainage can be substantial by minimizing the amount chloride-laden water from ponding inside the box beams, and thus, reducing the corrosion of steel reinforcement located in the bottom of the beams. This minimal effort should prevent much costlier future maintenance and extend the service life of the structure.

ACKNOWLEDGEMENTS

The authors gratefully acknowledge the guidance and assistance of Michael Sprinkel, Soundar Balakumaran, and Bernie Kassner of the Virginia Transportation Research Council. The assistance of David Mokarem, Brett Farmer, and Dennis Huffman at the Murray Structural Engineering Laboratory at Virginia Tech is also gratefully acknowledged.

REFERENCES

American Association of State Highway and Transportation Officials, *LRFD Bridge Design Specifications*. AASHTO, Washington, D.C., 2014.

ASTM. *Standard Test Methods for Testing Multi-Wire Steel Prestressing Strand.* ASTM A1061, West Conshohocken, PA, 2009.

ASTM. *Standard Test Method for Acid-Soluble Chloride in Mortar and Concrete*. ASTM C1152, West Conshohocken, PA, 2012.

ASTM. *Standard Test Method for Compressive Strength of Cylindrical Concrete Specimens*. ASTM C39, West Conshohocken, PA, 2005.

ASTM. *Standard Test Method for Obtaining and Testing Drilled Cores and Sawed Beams of Concrete*. ASTM C42, West Conshohocken, PA, 2016.

ASTM. *Standard Test Method for Half-Cell Potentials of Uncoated Reinforcing Steel in Concrete.* ASTM C876, West Conshohocken, PA, 2015.

ASTM. *Standard Test Method for Testing Multi-Wire Steel Prestressing Strand.* ASTM C876, West Conshohocken, PA, 2016.

Broomfield, John P. *Corrosion of Steel in Concrete*. Tylor & Francis, London, 2007.

Halbe, K. R. *New Approach to Connections between Members of Adjacent Box Beam Bridges*. Virginia Polytechnic Institute and State University, Blacksburg, VA, 2014.

Harries, K.A. Structural Testing of Prestressed Concrete Girders from Lake View Drive Bridge. *ASCE Journal of Bridge Engineering*, Vol. 14, No. 2, March/April 2009, pp.78-91.

Naito, C., Sause, R., Hodgson, I., Pessiki, S., and Macioce, T. Forensic Examination of a Noncomposite Adjacent Precast Prestressed Concrete Box Beam Bridge. *ASCE Journal of Bridge Engineering*, Vol. 15, No. 4, July/August 2010, pp. 408-418.

Naito, C., Jones, L., and Hodgson, I. Development of Flexural Strength Rating Procedures for Adjacent Prestressed Concrete Box Girder Bridges. *ASCE Journal of Bridge Engineering*, Vol. 61, No. 5, Sept/Oct 2011, pp. 662-670.

Naito, C., Jones, L., and Hodgson, I. *Inspection methods and techniques to determine non visible corrosion of prestressing strands in concrete bridge components: task 3, forensic evaluation and rating methodology*. ATLSS Report No. 09-10, Lehigh University, Bethlehem, PA, 2010.

Rogers, R., Wotherspoon, L., Scott, A. N., and Ingham, J. M. Residual Strength Assessment and Destructive Testing of Decommissioned Concrete Bridge Beams with Corroded Pretensioned Reinforcement. *PCI Journal*, Vol. 57, No. 3, Summer 2012, pp. 100-118.

APPENDIX A

Damage Quantification

This appendix describes the method used for damage quantification and provides one sample calculation.

In the first step, each type of damage was quantified and summed for each beam; no calculations were made except the summation of damage for each beam. Table A-1 presents the damage for each beam.

Table A-1. Quantification of Damage on Lesner Bridge Beams

Girder #	Girder Designation on Bridge	Total Long. Cracking (in)	Total Amount of Section Loss (in^2)	Total Amount of Delaminated Area (in^2)	Total Amount of Patched Area (in^2)
I-Beam 1	Span 22 Beam 5	56	120	48	96
I-Beam 2	Span 7 Beam 2	17	24	0	120
I-Beam 3	Span 19 Beam 4	90	147	138	0
I-Beam 4	Span 22 Beam 2	51	108	36	132
I-Beam 5	Span 19 Beam 2	130	66	231	0
I-Beam 6	Span 11 Beam 3	64	36	9	240
I-Beam 7	Span 13 Beam 5	0	0	0	0
I-Beam 8	Span 7 Beam 4	0	51	0	108
I-Beam 9	Span 5 Beam 2	83	48	132	0

In the second step, a percentage damage value was calculated by comparing the given defect value of a beam to the worst defect value of all the beams.

$$Damage\ \% = 100 * (1 - \frac{Given\ Girder\ Measured\ Value}{Worst\ Girder\ Measured\ Value})$$

Sample calculation for I-Beam 6:

$$Damage\ \%_{I-Beam\ 6-Total\ Long.\ Cracking} = 100 * \left(1 - \frac{64}{130}\right) = 50.8\%$$

$$Damage\ \%_{I-Beam\ 6-Total\ Amount\ of\ Section\ Loss} = 100 * \left(1 - \frac{36}{147}\right) = 75.5\%$$

$$Damage\ \%_{I-Beam\ 6-Total\ Amount\ of\ Delaminted\ Area} = 100 * \left(1 - \frac{9}{231}\right) = 96.1\%$$

$$Damage\ \%_{I-Beam\ 6-Total\ Amount\ of\ Patched\ Area} = 100 * \left(1 - \frac{240}{240}\right) = 0\%$$

The results of these calculations for all Lesner Bridge beams are shown in Table A-2.

Table A-2. Percent Damage of Lesner Bridge Beams

Girder #	Total Long. Cracking	Total Amount of Section Loss	Total Amount of Delaminated Area	Total Amount of Patched Area
I-Beam 1	56.9	18.4	79.2	60.0
I-Beam 2	86.9	83.7	100.0	50.0
I-Beam 3	30.8	0.0	40.3	100.0
I-Beam 4	60.8	26.5	84.4	45.0
I-Beam 5	0.0	55.1	0.0	100.0
I-Beam 6	50.8	75.5	96.1	0.0
I-Beam 7	100.0	100.0	100.0	100.0
I-Beam 8	100.0	65.3	100.0	55.0
I-Beam 9	36.2	67.3	42.9	100.0

In the final step, a weighting factor was applied to each type of damage and the weighted damage scores were summed to arrive at a final grade for each beam. An example calculation is shown below, and all beam scores are presented in Table A-3.

Sample calculation for I-Beam 6:

$$Final\ Grade\ \%_{I-Beam\ 6-Total\ Long.\ Cracking} = 50.8\% * (.3) = 15.24\%$$

$$Final\ Grade\ \%_{I-Beam\ 6-Total\ Amount\ of\ Section\ Loss} = 75.5\% * (.35) = 26.4\%$$

$$Final\ Grade\ \%_{I-Beam\ 6-Total\ Amount\ of\ Delaminated\ Area} = 96.1\% * (.25) = 24.0\%$$

$$Final\ Grade\ \%_{I-Beam\ 6-Total\ Amount\ of\ Patched\ Area} = 0\% * (.15) = 0\%$$

$$Final\ Grade\ \%_{I-Beam\ 6-Sum} = 15.24\% + 26.4\% + 24.0\% + 0\% = 65.64\%$$

Table A-3. Final Damage Rating for Lesner Bridge Beams

Girder #	Total Long. Cracking	Total Amount of Section Loss	Total Amount of Delaminated Area	Total Amount of Patched Area	Score
I-Beam 1	17.1	6.4	15.8	9.0	48.3
I-Beam 2	26.1	29.3	20.0	7.5	82.9
I-Beam 3	9.2	0.0	8.1	15.0	32.3
I-Beam 4	18.2	9.3	16.9	6.8	51.1
I-Beam 5	0.0	19.3	0.0	15.0	34.3
I-Beam 6	15.2	26.4	19.2	0.0	60.9
I-Beam 7	30.0	35.0	20.0	15.0	100.0
I-Beam 8	30.0	22.9	20.0	8.3	81.1
I-Beam 9	10.8	23.6	8.6	15.0	58.0